



Elisabeth Sattlegger, BSc

**A contribution to the determination  
of tunnel face instabilities in TBM tunnelling  
based on block theory**

**Master's Thesis**

Submitted in fulfilment of the requirements for the degree of

Diplom-Ingenieurin

Master's programme Civil Engineering, Geotechnics and Hydraulics

at

**Graz University of Technology**

Supervisors

O.Univ.-Prof. Dipl.-Ing. Dr.mont. Wulf Schubert

Dipl.-Ing. Michael Rudolf Henzinger

Dipl.-Ing. Dr.techn. Markus Pötsch, 3GSM GmbH

Institute of Rock Mechanics and Tunnelling

Graz University of Technology

Graz, November 2016

# Affidavit

Ich erkläre an Eides statt, dass ich die vorliegende Arbeit selbstständig verfasst, andere als die angegebenen Quellen/Hilfsmittel nicht benutzt, und die den benutzten Quellen wörtlich und inhaltlich entnommenen Stellen als solche kenntlich gemacht habe. Das in TUGRAZonline hochgeladene Textdokument ist mit der vorliegenden Masterarbeit identisch.

I declare that I have authored this thesis independently, that I have not used other than the declared sources/resources, and that I have explicitly marked all material which has been quoted either literally or by content from the used sources. The text document uploaded to TUGRAZonline is identical to the present master's thesis.

---

Datum / Date

---

Unterschrift / Signature

# Principle of equality

Due to reasons of legibility, this work does not include gender-specific formulations. However, the used male expressions stand for both genders.

# Danksagung

Beginnen möchte ich mit einem großen Dankeschön an Markus Pötsch, der die Idee für diese Masterarbeit lieferte und ohne den ich keine Chance gehabt hätte die Arbeit zu realisieren. Herzlichen Dank auch meinem Betreuer Michael Henzinger dafür, dass er sich immer Zeit genommen hat und Andreas Buyer, der mir bei den 3DEC-Simulationen geholfen hat. Weiters möchte ich Herrn Professor Wulf Schubert danken, der in seinen Vorlesungen mein Interesse für den Tunnelbau geweckt hat. Zusätzlich möchte ich Andreas Gaich einen Dank aussprechen, dass ich bei der 3GSM die 3D-Ringe erstellen konnte.

Ich möchte mich auch bei den Menschen in meinem Leben bedanken, die mich hierher gebracht haben und ohne die ich den Abschluss nicht geschafft hätte. Zuerst natürlich ein riesiges Dankeschön an meine Eltern Angelika und Martin. Hier kann der Dank nicht annähernd in Worte gefasst werden und ein Satz reicht hier bei weitem nicht aus. Danke auch meinem Bruder Martin, der mir der ehrlichste Mensch überhaupt ist. Auch erwähnen möchte ich meine Großeltern. Ich bin in der glücklichen Situation bei meiner Sponson noch alle vier bei mir zu haben. Dafür bin ich sehr dankbar.

Dankeschön auch allen Mitgliedern des Beton- und Holzbauzeichensaales und auch denen, die mittlerweile Veteranen sind - im Besonderen Staude, July, Magda und Gerhard. Abgesehen davon, dass die Mitgliedschaft mein Studium wesentlich vereinfacht hat, habe ich hier Freunde fürs Leben gefunden - Wake up.

Danke meiner WG (Gitte und Julia), die immer ein offenes Ohr für mich haben. Dies gilt auch für Rita bei der ich viel Studienstress abladen konnte.

Einen großen Beitrag zu dieser Diplomarbeit haben auch alle anderen Diplomanden im Diplomandenkammerl geleistet. Danke für eure Unterstützung und die nette Zeit im Kammerl.

Zusätzlich möchte ich meiner Mama und Andrew Thorn für das Korrigieren dieser Arbeit danken.

# Abstract

This master's thesis deals with the assessment of instabilities in a tunnel face when excavating with a tunnel boring machine (TBM). With the aid of a 3D tunnel face documentation moulds of detached blocks are localized within the tunnel face and their failure behaviour is analysed in terms of sliding and rotation.

The 3D tunnel face documentation is created by the system ShapeMetriXTBM (3GSM, 2016) developed by the 3GSM company. It was successfully applied within the framework of a research project by the ÖBB-Infrastruktur AG at the construction site of the Koralm Tunnel - lot KAT2, during which 20 three-dimensional tunnel face images were generated.

The images show moulds of detached blocks in the tunnel face, their failure behaviour however is unknown. For this reason a vector analysis based on block theory was conducted to determine whether the blocks may exhibit instabilities due to sliding or rotation. The basis for this calculation was provided by the work of Goodman & Shi (1985) and Tonon (1998) who developed a vector analysis of keyblock movements based on block theory.

As a basic assumption the analysed blocks are supposed to be tetrahedral and rigid. The acting forces result from the dead weight of the block and the average force of a disk cutter. The motion due to sliding is determined in terms of single-face sliding and double-face sliding. The motion due to rotation is determined around a corner and around an edge.

The vector analysis of the blocks was determined analytically with the software MATLAB (MathWorks, 2016). Additionally, the blocks were evaluated by a numerical simulation in 3DEC (Itasca, 2013). The comparison between the simulations displays little discrepancies. The numerical simulation shows a more realistic behaviour since it is possible to combine sliding and rotation. The method allows a better understanding of failure modes in a tunnel face.

# Kurzfassung

Im Zuge dieser Diplomarbeit wurden Instabilitäten in der Ortsbrust beim Vortrieb mit einer Tunnelbohrmaschine (TBM) untersucht. Mit Hilfe einer dreidimensionalen Ortsbrustdokumentation wurden einzelne Blockausbrüche in der Ortsbrust lokalisiert und anschließend das Versagen der Blöcke unter Verwendung einer Vektoranalyse berechnet.

Die dreidimensionale Ortsbrustdokumentation wurde mit dem System ShapeMetriXTBM (3GSM, 2016) der Firma 3GSM erstellt. Im Zuge einer Forschungsaktivität der ÖBB-Infrastruktur AG wurde diese Art der Ortsbrustdokumentation auf der Baustelle des Koralm-tunnels - Baulos KAT2 angewendet. Dafür wurden 20 Ortsbrustaufnahmen in 3D Bilder verarbeitet. Auf den Bildern sind Ortsbrustausbrüche klar ersichtlich und die Ausbrüche können bezüglich ihrer Position genau dokumentiert werden. Die Bilder lassen jedoch keine Rückschlüsse auf die Versagensart der Ausbruchblöcke zu.

Aus diesem Grund wurde das Versagen der Blöcke mit einer Vektoranalyse, basierend auf den Grundlagen der Blocktheorie genauer untersucht. Die Grundlage für die Berechnung liefert die Arbeit von Goodman & Shi (1985) und Tonon (1998). Steife, tetraedrische Blöcke wurden hinsichtlich Gleiten entlang einer oder zweier Flächen bzw. Rotation um eine Ecke und um eine Kante analysiert. Zu den einwirkenden Kräften zählen das Eigengewicht des Blockes und die Kraft, die aus der Einwirkung des Meißels auf die freie Oberfläche des Blockes resultiert. Die Analyse erfolgte mit dem Programm MATLAB (MathWorks, 2016). Zusätzlich wurde das Verhalten der Blöcke mit dem Programm 3DEC (Itasca, 2013) numerisch simuliert.

Die analytische Vektormethode ermöglicht keine Kombination von Gleit- und Rotationsversagen, weshalb sie nur als Annäherung angesehen werden kann. Durch die bekannten Berechnungsbedingungen kann die Vektoranalyse für die Verifizierung der numerischen Simulation, welche realistische Ergebnisse liefert, herangezogen werden. Die Vektormethode hilft das Bruchverhalten in einer Ortsbrust beim Vortrieb mit einer Tunnelbohrmaschine besser zu verstehen.

---

# Contents

<b>1</b>	<b>Introduction</b>	<b>1</b>
1.1	State of the art . . . . .	1
1.2	Structure of the thesis . . . . .	2
1.3	Objectives . . . . .	3
<b>2</b>	<b>Method</b>	<b>4</b>
2.1	Tunnel face documentation with 3D images . . . . .	4
2.1.1	Advantages of digital tunnel face documentation . . . . .	4
2.1.2	Installation of the imaging unit . . . . .	5
2.1.2.1	Hardware equipment . . . . .	5
2.1.2.2	Documentation procedure . . . . .	6
2.1.3	Generation of a 3D image . . . . .	7
2.1.3.1	Software equipment . . . . .	7
2.1.3.2	Generation of the 3D image . . . . .	7
2.1.4	Analysis of a 3D image . . . . .	10
2.1.4.1	Geologic mapping . . . . .	10
2.1.4.2	Geometric measurement . . . . .	10
2.1.5	Application at the construction site of KAT2 . . . . .	12
2.2	Block theory for tunnel face instabilities . . . . .	14
2.2.1	Introduction to block theory . . . . .	14
2.2.2	Description of the block geometry using vector methods . . . . .	15
2.2.3	Active forces . . . . .	17
2.2.4	Vector analysis of translations . . . . .	19
2.2.4.1	Single-face sliding . . . . .	19
2.2.4.2	Double-face sliding . . . . .	21
2.2.5	Vector analysis of rotations . . . . .	21
2.2.5.1	Mode analysis . . . . .	22

---

2.2.5.2	Stability analysis . . . . .	27
2.3	Numerical analysis of tunnel face instabilities . . . . .	30
<b>3</b>	<b>Block stability analysis using analytical and numerical methods</b>	<b>31</b>
3.1	Results of block theory . . . . .	31
3.1.1	Corner rotation . . . . .	32
3.1.2	Edge rotation . . . . .	33
3.2	Numerical simulation of block failure in 3DEC (Itasca, 2013) . . . . .	36
3.2.1	Corner rotation in 3DEC (Itasca, 2013) . . . . .	36
3.2.2	Edge rotation in 3DEC (Itasca, 2013) . . . . .	38
3.3	Case study based on the 3D tunnel face documentation . . . . .	40
3.3.1	Tunnel face at chainage 14321.13 m . . . . .	40
3.3.2	Tunnel face at chainage 14335.46 m . . . . .	42
3.3.3	Tunnel face at chainage 14660.39 m . . . . .	43
3.3.4	Tunnel face at chainage 14703.07 m . . . . .	46
<b>4</b>	<b>Conclusion and Outlook</b>	<b>48</b>

## List of Figures

1.1	Documentation of a tunnel face at KAT2 . . . . .	2
2.1	Imaging unit with smartphone, outdoor camera, LED lamps and laser pointers	5
2.2	Subimage of the video showing a detail of the tunnel face and parts of the inspection opening in the border areas . . . . .	6
2.3	Functionality of the 3D generation with overlapping images (Irschara et al., 2011) . . . . .	8
2.4	Sparse 3D point cloud of an annular tunnel face image with associated camera positions . . . . .	9
2.5	Final 3D image with associated camera positions . . . . .	10
2.6	Topographic map for illustrating the depth of block detachments . . . . .	11
2.7	Visualisation of the cut-off plane with fraction in front and behind the plane	12
2.8	Overview of the construction site at the Koralm Tunnel (Harer et al., 2008) .	12
2.9	Single-face sliding . . . . .	20
2.10	Relationship between the sliding direction and the normal vectors of the bordering planes . . . . .	20
2.11	Double-face sliding . . . . .	21
2.12	Corner rotation around the upper corner . . . . .	23
2.13	Relationship between the joint planes defined by the normal vectors . . . . .	23
2.14	Relationship between normal vectors changes if the angle between the joint planes changes . . . . .	24
2.15	Conditions for corner rotation around corner $A_i$ . . . . .	25
2.16	Edge rotation with rotation axis in an edge . . . . .	26
2.17	Conditions for edge rotation around the corners $A_i$ and $A_j$ . . . . .	27
3.1	Ideal block shape for corner rotation with an applied cutter force of 200 kN .	32
3.2	Cutter head of the TBM at KAT2 and block for the rotation analysis . . . . .	33

---

3.3	Ideal block shape for edge rotation . . . . .	34
3.4	Edge rotation depends on the acting direction of the cutter force . . . . .	35
3.5	State of equilibrium with the acting forces . . . . .	35
3.6	Ideal block for corner rotation highlighted in red . . . . .	36
3.7	Rotation around the upper corner . . . . .	37
3.8	Ideal block for edge rotation highlighted in yellow . . . . .	38
3.9	Rotation around the upper edge . . . . .	39
3.10	3D image of the tunnel face at chainage 14321.13 m and topographic map of the tunnel face with the detached block highlighted in red . . . . .	40
3.11	Analysis of a tetrahedral block at chainage 14321.13 m . . . . .	41
3.12	Numerical simulation of a tetrahedral block (red) at chainage 14321.13 m . .	41
3.13	3D image of the tunnel face at chainage 14335.46 m and topographic map of the tunnel face with the detached block highlighted in red . . . . .	42
3.14	Analysis of a tetrahedral block at chainage 14335.46 m . . . . .	43
3.15	Numerical simulation of a tetrahedral block (pink) at chainage 14335.46 m . .	43
3.16	3D image of the tunnel face at chainage 14660.39 m and topographic map of the tunnel face with the detached block highlighted in red . . . . .	44
3.17	Analysis of a tetrahedral block at chainage 14660.39 m . . . . .	45
3.18	Numerical simulation of a tetrahedral block (yellow) at chainage 14660.39 m .	45
3.19	3D image of the tunnel face at chainage 14703.07 m and topographic map of the tunnel face with the detached block highlighted in red . . . . .	46
3.20	Analysis of a tetrahedral block at chainage 14703.07 m . . . . .	47
3.21	Numerical simulation of a tetrahedral block (red) at chainage 14703.07 . . . .	47

## Symbols

$a, b, c$	.....	moments of inertia
$a', b', c'$	.....	products of inertia
$a_f$	.....	distance between centroid and point of application of the active force
$a_G$	.....	translational acceleration
$A_i$	.....	vertex
$\gamma$	.....	unit weight
$\mathbf{E}$	.....	inertia operator
$F$	.....	cutter force
$f$	.....	acting point of cutter force
$\phi$	.....	friction angle
$G$	.....	dead weight of the block
$g$	.....	centroid of the block
$I_{ij}$	.....	intersection of two planes
$m$	.....	mass
$M_g$	.....	moment relative to the centroid $g$
$M_{A_i}$	.....	moment around corner $A_i$
$\hat{n}_i$	.....	normal vector of a plane
$P$	.....	frictional resistance
$R$	.....	resultant force
$\hat{s}_i$	.....	sliding direction
$V$	.....	volume of the block
$X_i, Y_i, Z_i$	.....	coordinates of the normal vector
$\dot{\omega}$	.....	angular acceleration

# 1 Introduction

## 1.1 State of the art

When excavating a tunnel with a tunnel boring machine (TBM) the assessment and the geological mapping of the tunnel face is much more challenging compared to conventional tunnelling. The inspection openings are the only possibility to observe the tunnel face during maintenance shifts. Often the openings are barred due to detached blocks. The whole analysis of the tunnel face is based on estimates.

Usually the geologist observes and takes pictures of the tunnel face through the inspection openings. Afterwards the tunnel face documentation is drawn which could lead to inconsistencies due to the fact that the dimensions of fault zones and inclusions are difficult to identify from the inspection openings. Furthermore, there is a period of time between observing the tunnel face and drawing the tunnel face documentation. Hence important information could be missed.

In fault zones the access to the tunnel face is further limited because blocks which fell down can limit the visibility. Furthermore the inspection through the opening is dangerous while the TBM excavates in a fault zone because rock falls might occur.

The tunnel face documentation consists of a drawing of the tunnel face where foliations, joint planes, slickensides and fault zones are mapped. Furthermore the documentation includes information about the plunge and trend of the joint planes, slickensides, etc. and details about the system behaviour and the rock type.

Figure 1.1 shows a typical tunnel face documentation with its foliations, joint planes and slickensides.

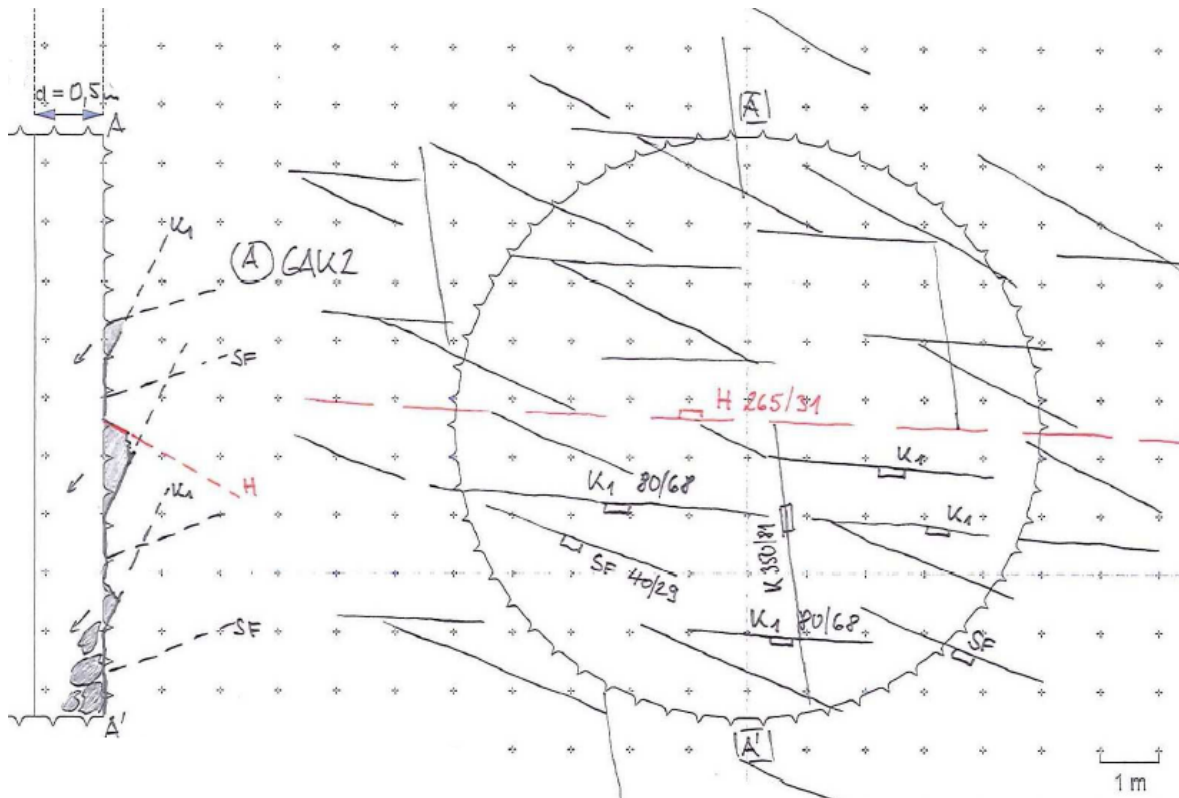


Figure 1.1: Documentation of a tunnel face at KAT2

## 1.2 Structure of the thesis

Chapter 2 starts with 3D tunnel face documentation, describing the installation of an imaging unit in the inspection opening, the generation of a 3D image and the possibilities to analyse the 3D image in terms of geological mapping and geometric measurements. In addition the application at the construction site is mentioned. Furthermore, the thesis describes the basics of block theory and how it can be applied for determining the behaviour of a block when loaded by a disk from the cutter head of the TBM.

The main part of the thesis contains the determination of the possibility for rotational failure. Subsequently the block behaviour was calculated for the detached blocks from the 3D tunnel face documentation of KAT2. Tetrahedral blocks from the 3D images were analysed with the help of a vector analysis based on block theory in MATLAB (MathWorks, 2016) and afterwards a numerical simulation was carried out in 3DEC (Itasca, 2013).

The thesis concludes with a discussion of the results of the analytical and numerical computation. Furthermore the significance of the results is explained.

### 1.3 Objectives

Previous papers and calculations by Goodman & Shi (1985), Tonon (1998) and others considered the block weight and applied forces like anchor forces, etc. for the determination of failure modes. Subsequently block failure occurs in terms of lifting or sliding along one or two joint planes. Rotation is a rare mode of failure.

This thesis introduces the concept of a cutter force penetrating the tunnel face. This force acts into the rock mass and stabilizes the block against sliding although it favours rotational instability. Therefore the thesis **investigates the influence of eccentric forces** on the stability of blocks.

The method based on vector analysis is verified and it is possible to **gain a new understanding of failure modes in a tunnel face** when excavating with a TBM.

## 2 Method

### 2.1 Tunnel face documentation with 3D images

To provide a successful and economic tunnel project sufficient information about the ground conditions is necessary. In conventional tunnelling the entire tunnel face is visible after each blast. Therefore geologists and engineers can gather information on the rock mass structure. The geologists are able to get a comprehensive overview of the tunnel face because all areas are visible.

In contrast to conventional tunnelling a TBM allows only a limited view on the tunnel face through inspection openings. This fact prohibits a complete determination of the rock mass conditions. The 3GSM company developed a concept for face documentation for TBMs by installing a camera in one or several of the inspection openings in order to record a video of the tunnel face. From this video a 3D image is created using software called ShapeMetriXTBM (3GSM, 2016). This video can then be analysed on a computer. The complete approach for installing the unit, generating a 3D image and analyzing this image is described by Gaich & Pötsch (2016).

#### 2.1.1 Advantages of digital tunnel face documentation

The 3D image is composed of a three-dimensional visualization with geometrical information. In this way areas that are normally not visible can be covered. The analysis is carried out numerically, where several evaluation tools are available. It is a safe and accurate way of documenting the tunnel face. With the adequate software the quantification of moulds of detached blocks, geological mapping as well as predictions of the face planarity are possible.

A video is taken from an inspection opening. A 3D circular ring image that covers approximately 30-40 percent of the tunnel face is produced. The coverage depends on the distance between the cutter head and the tunnel face. In another test series the imaging unit was

installed in foam contraction chokes which are spread over the cutter head. This allowed the recording of several rings for a holistic 3D image of the tunnel face.

## 2.1.2 Installation of the imaging unit

### 2.1.2.1 Hardware equipment

The imaging unit consists of an outdoor camera and its dust-proof housing, an Android smartphone, which is connected with the camera via WiFi, LED lamps at the right and left side of the camera and a pair of laser pointers used for scaling purposes. All components are fixed to an aluminium frame (see figure 2.1).



Figure 2.1: Imaging unit with smartphone, outdoor camera, LED lamps and laser pointers

At the front side of the imaging unit the outdoor camera is fixed and protected by a dust proof housing. This camera records the video. The smartphone is positioned at the back of the unit, controls the camera and records the orientation of the system. The LED lamps provide autonomous lighting to ensure appropriate illumination of the face. The lights run with low power consumption to facilitate small and easily transportable batteries. In addition two laser pointers provide scale information since the two points can be seen on the video. Therefore the user is able to get an impression of the distance from the camera to the tunnel face. The individual components are mounted to a self-standing frame with two fixed magnetic feet and one movable foot for adjusting the unit. The frame size is based on a circular inspection opening with a diameter of 62 cm.

### 2.1.2.2 Documentation procedure

The installation takes place during the maintenance shift in one of the inspection openings in the cutter head of the tunnel boring machine. To achieve optimum results the unit has to be fixed in a way that the camera is placed horizontally to receive landscape images. The width of the taken video depends on the distance between camera and tunnel face. Therefore the cutter head should be retracted if conditions allow it. In this application the face has additionally been washed in order to enhance the visibility of geologic features. Otherwise, dust may compromise the recorded pictures.

After mounting the unit, switching on the LED lights and activating the camera with the App of the smartphone the user needs to leave the hazard area. Afterwards the cutter head rotates by at least 360°. While the head turns the camera is recording a circular ring video of the tunnel face and the phone records the scaling data. Figure 2.2 shows a single image of the tunnel face and parts of the inspection opening at the border areas.



Figure 2.2: Subimage of the video showing a detail of the tunnel face and parts of the inspection opening in the border areas

After the tunnel boring machine halts the user stops the recording by using the App on the smartphone and then removes the unit from the inspection opening. The user needs the memory card of the camera and the orientation data from the smartphone for data processing. The whole recording process including mounting and demounting of the unit

takes approximately five minutes.

### 2.1.3 Generation of a 3D image

The 3GSM company developed a software product called ShapeMetriXTBM (3GSM, 2016) which consists of several modules for generating and analysing the three-dimensional tunnel face images.

#### 2.1.3.1 Software equipment

For the creation of the 3D image ShapeMetriXTBM (3GSM, 2016) uses three main components:

- TBM ProjectCreator: This component extracts a series of pictures from the video and removes useless information.
- TBM Multiphoto: The Multiphoto component is a photogrammetric reconstruction module which enables the further processing of a huge amount of highly redundant pictures. This component generates the final 3D image and references it.
- JMX Analyst: This module allows viewing and analysing the 3D image. It is possible to determine the size of block detachment as well as joint orientation.

#### 2.1.3.2 Generation of the 3D image

The video is loaded into the TBM ProjectCreator software. With the software it is possible to select an adequate quantity of image frames. The images need sufficient overlap to ensure that each point is visible in at least two image frames. Figure 2.3 shows the functionality for overlapping the single subimages. The images are all taken from an equal distance from the tunnel face. Any irregular rotational speeds and stops can be compensated.

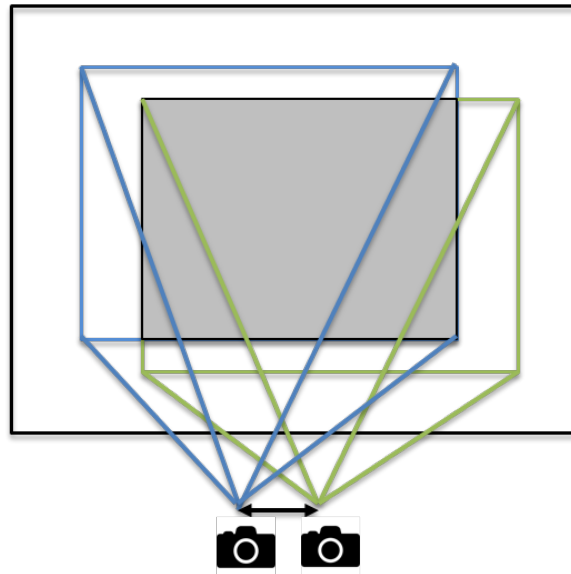


Figure 2.3: Functionality of the 3D generation with overlapping images (Irschara et al., 2011)

Occasionally the inspection opening is visible on the video, depending on the mounting position of the unit. For this reason the software contains a tool to delete all static borders.

Additionally an xml-file is generated from the smartphone data which includes information about the chainage, camera installation radius, camera identification and the coordinates and angles of each picture. This xml-file is necessary for the further registration.

Next, highly overlapping pictures are loaded into the TBM MultiPhoto software from where the reconstruction is created in several steps. A Structure-from-Motion-concept (SfM) (Irschara et al., 2011) was applied, meaning that a series of steps can assimilate a huge amount of unordered but redundant pictures. All camera locations are determined by solving a linear system of equations and thus enabling an optimised result for the given camera.

After that a point cloud with numerous individual sparse 3D points is generated from the single images. Figure 2.4 shows the point cloud of a 3D ring image.

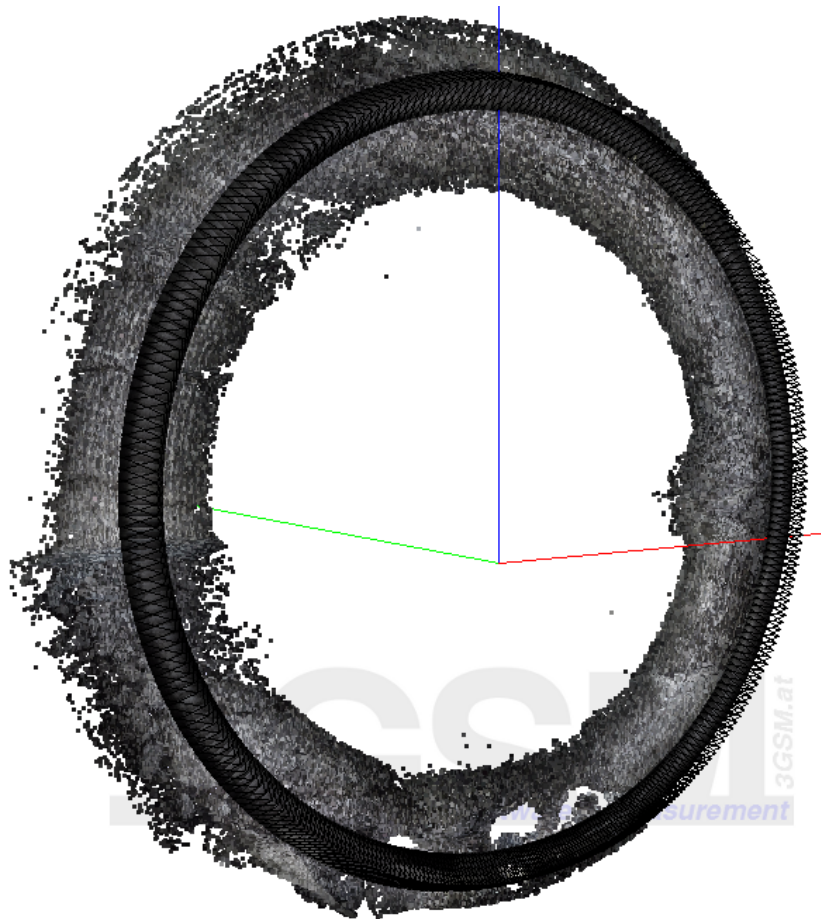


Figure 2.4: Sparse 3D point cloud of an annular tunnel face image with associated camera positions

The software then extracts similar points in two different pictures and creates a pair of the two pictures. The pairs are chosen automatically by the software and the entire recorded area is covered with 3D image pairs. Afterwards these pairs are used to create a single 3D image. The result is a 3D ring image, which allows a view of the tunnel face and is used for relative measurements.

Scale and orientation data is included in the processing pipeline to allow the referencing of the 3D image in terms of north and east direction and the azimuth is also defined.

Figure 2.5 shows the final 3D ring with the associated camera positions.



Figure 2.5: Final 3D image with associated camera positions

#### 2.1.4 Analysis of a 3D image

Besides the visual aspects of a 3D image it also includes geometric data. A variety of parameters is determinable, such as information about the joint sets, fracture surfaces and the planarity and quality of the tunnel face in general.

##### 2.1.4.1 Geologic mapping

The generated 3D image facilitates geologic mapping. The user can identify the number of joint sets, joint set spacing and joint frequency, orientations, size, location and shape from fracture surfaces and traces, aperture, roughness and the volume of single blocks.

##### 2.1.4.2 Geometric measurement

The software creates a reference plane in the ideal tunnel face and allows assessment of all deviations that are located behind this plane. For blocks it is possible to estimate the volume in  $m^3$  by outlining the borders of the block with a polygon and its depth. The depth of single

block detachments can be shown in a topographic map (see figure 2.6). The user can define the maximum depth and the step sizes for the coloring.

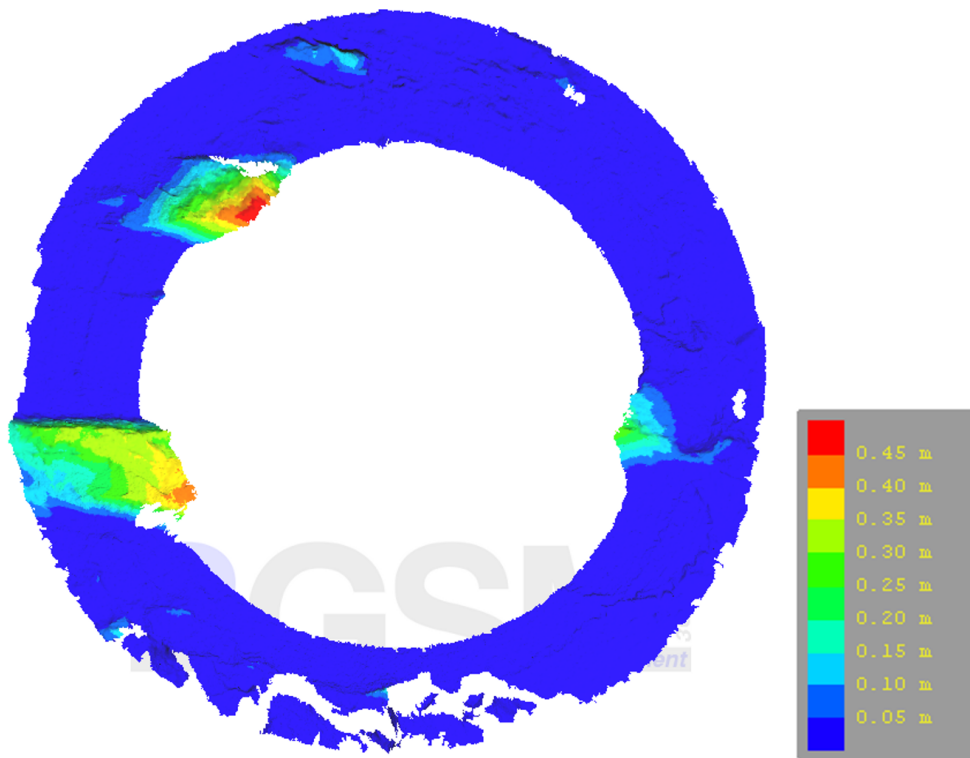


Figure 2.6: Topographic map for illustrating the depth of block detachments

Additionally the planarity of the tunnel face can be described by a so called cut-off plane which is parallel to the reference plane. The cut-off plane can be relocated along its normal. The software distinguishes between rock mass in front of the plane and behind the plane and indicates the amount in percent and  $m^2$ . Subsequently quantifications like the fraction that exceeds a certain overbreak depth are possible (see figure 2.7).

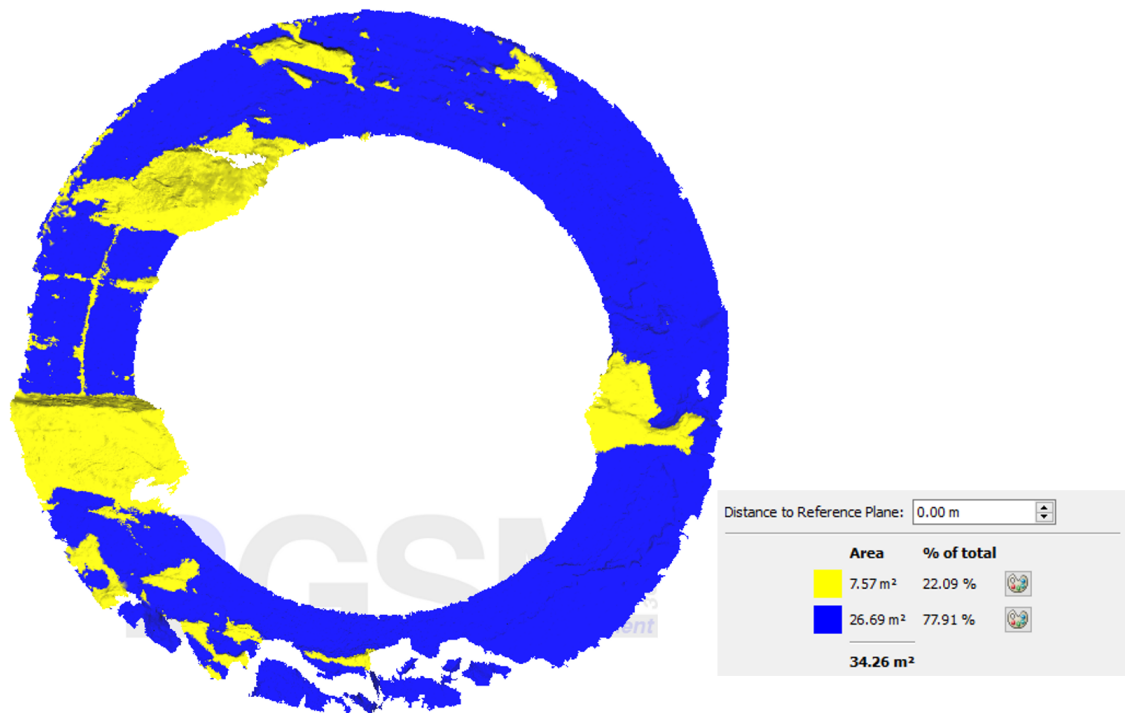


Figure 2.7: Visualisation of the cut-off plane with fraction in front and behind the plane

### 2.1.5 Application at the construction site of KAT2

The imaging unit and the software have been successfully applied at the construction site of the Koralm Tunnel. Two tunnel boring machines are used at the construction section KAT2 in Styria. Figure 2.8 shows an overview of the construction site.

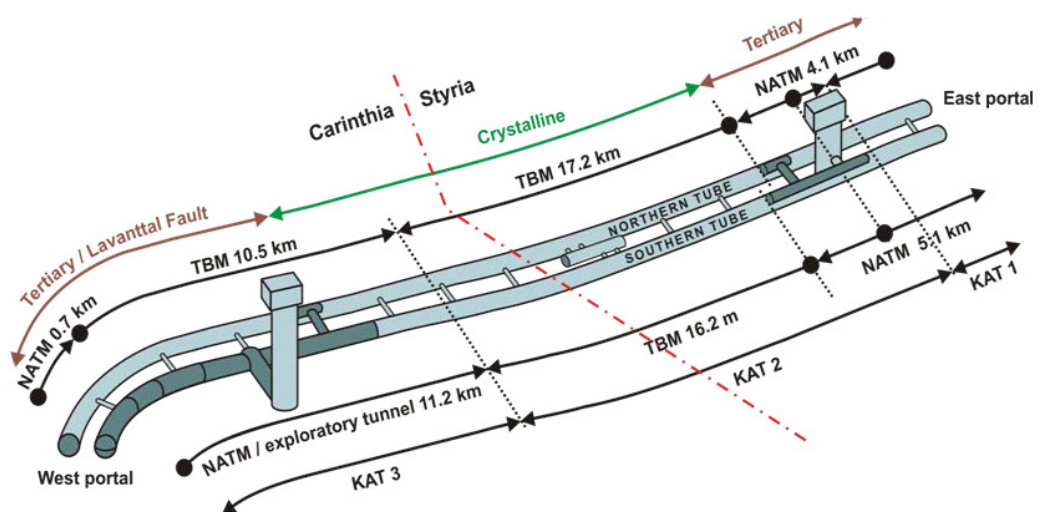


Figure 2.8: Overview of the construction site at the Koralm Tunnel (Harer et al., 2008)

---

After initial attempts in spring 2015 a full scale test run was started in March 2016. The geologists took 20 videos during the daily maintenance shifts and were able to extract the overlapping single images using the TBM ProjectCreator software. The pictures and the simultaneously created orientation file were transmitted to the 3GSM company. The data packets with the image frames were utilised to create 20 three-dimensional tunnel face images with the use of the TBM MultiPhoto software which were then sent back to the geologists at the construction site.

The generated images were analysed in regard to the instabilities in the tunnel face and used for the case study to determine the failure modes of the detached blocks. Chapter 3 shows several investigated tunnel faces and the results of the calculation.

## 2.2 Block theory for tunnel face instabilities

### 2.2.1 Introduction to block theory

With the help of block theory it is possible to analyse a system of discontinuities to localise the critical key block along an excavated surface in three dimensions. The analysis proves to be ideal for hard, blocky rock and can be applied either by graphical representation or vector methods. This thesis analyses the blocks by vector methods. The use of vector analysis in block theory allows kinematic and static equilibrium analysis of key blocks under the influence of the dead weight and applied forces like the cutter force.

The calculation routine presented in this master's thesis is mainly based on the work by Goodman & Shi (1985), Tonon (1998) and Pötsch (2011). In "Block theory and its application to rock engineering" Goodman & Shi (1985) provide the basis for block theory and the possible failure modes. In his paper "Generalization of Mauldon's and Goodman's vector analysis of keyblock rotations" Tonon (1998) describes the stability of blocks against translation and rotation. In his doctoral thesis "The analysis of rotational and sliding modes of failure for slopes, foundations, and underground structures in blocky, hard rock" Pötsch (2011) defines a procedure for integrating discontinuity measurements from 3D images into a block analysis method.

The analysis is based on the following assumptions:

- All blocks are tetrahedral - three joint planes are located in the rock mass and one free face is located at the tunnel face.
- The joint surfaces and the free face are perfectly planar. This is necessary to describe the block morphology in terms of linear vector equations.
- All blocks are defined by pre-existing joints. New cracks are not taken into consideration and do not influence the calculation.
- All blocks are rigid.
- Cohesion and tensile strength of the joints are regarded negligible.
- At the beginning of the calculation the system is at rest. This is important for the assumed equations of motion as the angular velocity is equal to zero at the beginning of the motion.

In general block theory can be described as a method based on geometric information derived from geological parameters and equilibrium calculations by means of basic statics. Since the block is rigid, deformation and distortion will not be taken into consideration. Block theory is defined through geometry. Rotation and sliding are the only modes taken into account for this thesis. Failure due to lifting was not analysed. Failure due to erosion, formation of new cracks in the rock and flexure of layers are also not part of block theory.

A few input parameters are essential to start the calculation:

- Trend and plunge of the three joint planes and their normal distance from the origin which is located in the tunnel axis.
- Trend and plunge and normal distance of the tunnel face. Since the origin is located in the tunnel axis the trend is equal to zero, the plunge is  $90^\circ$  and the normal distance from the face to the origin is also equal to zero.
- Upper or lower halfspace of the joints indicates the direction of the normal vectors that have to point into the block.
- Unit weight of the rock mass
- Average cutter force of one cutter
- Contact point of the cutter force
- Friction angle of the joint planes

### 2.2.2 Description of the block geometry using vector methods

Vector analysis is a relatively simple approach to determine all quantities for describing a block, including the volume and the coordinates of the vertices. The block is described by the orientation of each joint plane defined by plunge (between  $0^\circ$ - $90^\circ$ ) and trend (between  $0^\circ$ - $360^\circ$ ). Usually the joint plane intersects with the horizontal xy-plane whereas for this thesis the trend indicates the relation to the tunnel axis and the plunge is defined as the inciding inclination of the joint plane. Usually the trend describes the relationship between the planes and the north direction. The normal vector  $\hat{n}_i$  is a unit vector and perpendicular to a plane. It consists of x-, y- and z-coordinates.

$$\hat{n}_i = (X_i, Y_i, Z_i) \quad (2.1)$$

The coordinates of the normal vector  $\hat{n}_i$  are defined by plunge ( $\alpha$ ) and trend ( $\beta$ ) with the help of the following equations:

$$\begin{aligned} X_i &= \sin(\alpha) \sin(\beta) \\ Y_i &= \sin(\alpha) \cos(\beta) \\ Z_i &= \cos(\alpha) \end{aligned} \tag{2.2}$$

The algebraic sign of the values depends on the pointing direction of the normal vector  $\hat{n}_i$  which must point into the block.

The edge of a block is formed by the intersection of two planes determined by the cross product of their normal vector.

$$I_{ij} = \hat{n}_i \times \hat{n}_j \tag{2.3}$$

The corner of a tetrahedral block is defined as the intersection of three planes and can be calculated by solving an equation system with three unknown values. If, for example, a vertex is formed by the intersection of plane 1, 2 and 3 the coordinates are determined by solving:

$$\begin{aligned} X_1x + Y_1y + Z_1z &= D_1 \\ X_2x + Y_2y + Z_2z &= D_2 \\ X_3x + Y_3y + Z_3z &= D_3 \end{aligned} \tag{2.4}$$

The distance of the normal vector from the origin to the plane is defined by the input parameter  $D$ .

A tetrahedral block consists of four vertices whereas three vertices are located at the tunnel face and one is located inside the rock mass. For a failure to occur the face vertices are not allowed to exceed the tunnel radius. Otherwise the block becomes infinite.

With the coordinates of the vertices it is possible to calculate the volume of the block.

$$V = \frac{1}{6} \begin{vmatrix} 1 & x_1 & y_1 & z_1 \\ 1 & x_2 & y_2 & z_2 \\ 1 & x_3 & y_3 & z_3 \\ 1 & x_4 & y_4 & z_4 \end{vmatrix} \quad (2.5)$$

The volume and the unit weight are used to calculate the mass of the tetrahedral block.

$$m = \gamma * V \quad (2.6)$$

### 2.2.3 Active forces

Two forces are considered. One force results from the dead weight of the block and the other force from the average normal disk force of each cutter. The resultant force R is composed of the dead weight G calculated from the mass of the block and the cutter force F.

$$R = (0, F, -G) \quad (2.7)$$

The dead weight G acts in the centroid with the following coordinates:

$$g = (x_g, y_g, z_g) \quad (2.8)$$

The coordinates of the centroid g can be determined with the coordinates of the block vertices.

$$\begin{aligned} x_g &= \frac{(x_1 + x_2 + x_3 + x_4)}{4} \\ y_g &= \frac{(y_1 + y_2 + y_3 + y_4)}{4} \\ z_g &= \frac{(z_1 + z_2 + z_3 + z_4)}{4} \end{aligned} \quad (2.9)$$

Additionally, the cutter force F acts in point f. It has to be mentioned that the coordinate  $y_f$  is zero because the cutter force acts at the free face where the origin is located.

$$f = (x_f, y_f, z_f) \quad (2.10)$$

The distance between centroid and acting point of the cutter force determines the eccentricity of the cutter force.

$$a_f = (x_g, y_g, z_g) - (x_f, y_f, z_f) \quad (2.11)$$

Furthermore the moment  $M_g$  relative to the centroid is defined as:

$$M_g = a_f \times F \quad (2.12)$$

It is necessary to calculate the distance between the vertices and the centroid as the origin is located in the centroid.

$$\begin{aligned} C_1 &= (x_1, y_1, z_1) = (x_1, y_1, z_1) - (x_G, y_G, z_G) \\ C_2 &= (x_2, y_2, z_2) = (x_2, y_2, z_2) - (x_G, y_G, z_G) \\ C_3 &= (x_3, y_3, z_3) = (x_3, y_3, z_3) - (x_G, y_G, z_G) \\ C_4 &= (x_4, y_4, z_4) = (x_4, y_4, z_4) - (x_G, y_G, z_G) \end{aligned} \quad (2.13)$$

The quantities a, b and c are the moments of inertia contingent on the axes x, y and z. They form the main diagonal of the inertia operator (Kuypers, 1997).

$$\begin{aligned} a &= \int_D \gamma(y^2 + z^2)dD = \gamma * |DET(J)| * (y_1^2 + y_1y_2 + y_2^2 + y_1y_3 + y_2y_3 + y_3^2 + y_1y_4 \\ &\quad + y_2y_4 + y_3y_4 + y_4^2 + z_1^2 + z_1z_2 + z_2^2 + z_1z_3 + z_2z_3 + z_3^2 + z_1z_4 + z_2z_4 + z_3z_4 + z_4^2/60 \\ b &= \int_D \gamma(x^2 + z^2)dD = \gamma * |DET(J)| * (x_1^2 + x_1x_2 + x_2^2 + x_1y_3 + x_2x_3 + x_3^2 + x_1x_4 \\ &\quad + x_2x_4 + x_3x_4 + x_4^2 + z_1^2 + z_1z_2 + z_2^2 + z_1z_3 + z_2z_3 + z_3^2 + z_1z_4 + z_2z_4 + z_3z_4 + z_4^2/60 \\ c &= \int_D \gamma(x^2 + y^2)dD = \gamma * |DET(J)| * (x_1^2 + x_1x_2 + x_2^2 + x_1y_3 + x_2x_3 + x_3^2 + x_1x_4 \\ &\quad + x_2x_4 + x_3x_4 + x_4^2 + y_1^2 + y_1y_2 + y_2^2 + y_1y_3 + y_2y_3 + y_3^2 + y_1y_4 + y_2y_4 + y_3y_4 + y_4^2/60 \end{aligned} \quad (2.14)$$

The secondary diagonal is formed by the products of inertia  $a'$ ,  $b'$  and  $c'$ .

$$\begin{aligned}
a' &= \int_D \gamma(yz) dD = \gamma * |DET(J)| * (2y_1z_1 + y_2z_1 + y_3z_1 + y_4z_1 + y_1z_2 + 2y_2z_2 + y_3z_2 \\
&\quad + y_4z_2 + y_1z_3 + y_2z_3 + 2y_3z_3 + y_4z_3 + y_1z_4 + y_2z_4 + y_3z_4 + 2y_4z_4/120 \\
b' &= \int_D \gamma(xz) dD = \gamma * |DET(J)| * (2x_1z_1 + x_2z_1 + x_3z_1 + x_4z_1 + x_1z_2 + 2x_2z_2 + x_3z_2 \\
&\quad + x_4z_2 + x_1z_3 + x_2z_3 + 2x_3z_3 + x_4z_3 + x_1z_4 + x_2z_4 + x_3z_4 + 2x_4z_4/120 \\
c' &= \int_D \gamma(xy) dD = \gamma * |DET(J)| * (2x_1y_1 + x_2y_1 + x_3y_1 + x_4y_1 + x_1y_2 + 2x_2y_2 + x_3y_2 \\
&\quad + x_4y_2 + x_1y_3 + x_2y_3 + 2x_3y_3 + x_4y_3 + x_1y_4 + x_2y_4 + x_3y_4 + 2x_4y_4/120
\end{aligned} \tag{2.15}$$

With the moments of inertia and the products of inertia it is possible to compute the inertia operator relative to the centroid.

$$\mathbf{E} = \begin{pmatrix} a & -b' & -c' \\ -b' & b & -a' \\ -c' & -a' & c \end{pmatrix} \tag{2.16}$$

## 2.2.4 Vector analysis of translations

The translational analysis deals with the relationship between the direction of the resultant force for a sliding block and its sliding direction.

Translational analysis is divided into single-face sliding and double-face sliding.

### 2.2.4.1 Single-face sliding

The block slides along one joint plane. The sliding direction  $\hat{s}_i$  is the orthographic projection of the resultant  $R$ . Figure 2.9 shows an example of single-face sliding along a joint plane for a tetrahedral block.

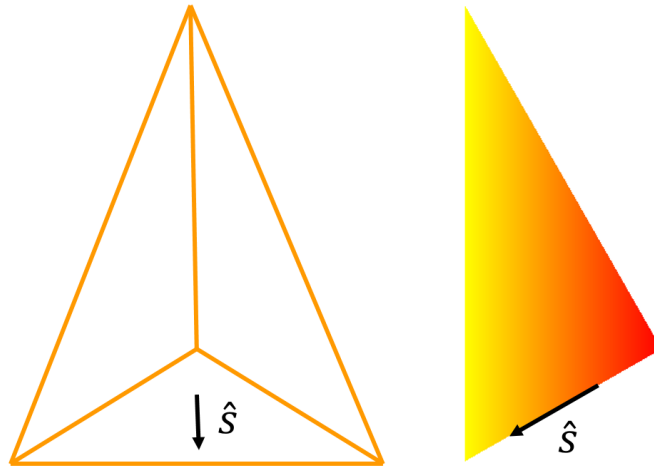


Figure 2.9: Single-face sliding

The sliding direction is calculated as follows:

$$\hat{s}_i = \frac{(\hat{n}_i \times R) \times \hat{n}_i}{|\hat{n}_i \times R|} \quad (2.17)$$

The relationship between the sliding direction and the normal vectors of the planes is shown on figure 2.10 and can be calculated with:

$$\hat{s}_i \cdot \hat{n}_h > 0 \text{ or } \hat{s}_i \cdot \hat{n}_j > 0 \quad (2.18)$$

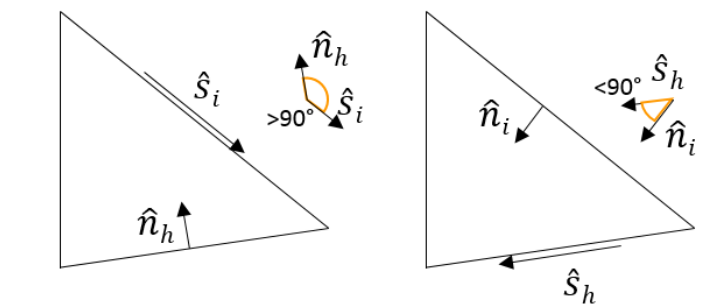


Figure 2.10: Relationship between the sliding direction and the normal vectors of the bordering planes

If the block is unstable in terms of sliding it might still be fixed to its position due to the friction angle. Since there is only one plane in contact with the rock mass according to Goodman & Shi (1985) the equation reads:

$$P = |\hat{n}_i \times R| - |\hat{n}_i \cdot R| \tan(\phi) < 0 \quad (2.19)$$

#### 2.2.4.2 Double-face sliding

The sliding direction  $\hat{s}_i$  for double-face sliding is parallel to the intersection of the two planes. The mode describes sliding on an inward edge of the block.

$$\hat{s}_i = \frac{\hat{n}_i \times \hat{n}_j}{|\hat{n}_i \times \hat{n}_j|} \text{sign}((\hat{n}_i \times \hat{n}_j) \cdot R) \quad (2.20)$$

Figure 2.11 shows an example of double-face sliding along an edge for a tetrahedral block.

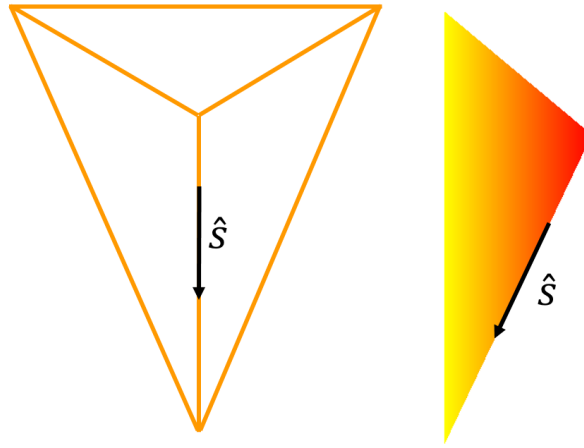


Figure 2.11: Double-face sliding

Goodman & Shi (1985) define the stability against friction on two joint planes as follows:

$$P = \frac{1}{(|\hat{n}_i \times \hat{n}_j|)^2} [ |R \cdot (\hat{n}_i \times \hat{n}_j)| |\hat{n}_i \times \hat{n}_j| - |(R \times \hat{n}_j) \cdot (\hat{n}_i \times \hat{n}_j)| \tan(\phi) ] < 0 \quad (2.21)$$

#### 2.2.5 Vector analysis of rotations

The vector analysis determines the rotational modes and the rotational stability. There are four kinds of rotation:

- Corner rotation: The rotation axis intersects at only one corner at the surface.
- Edge rotation: The rotation axis intersects with two free corners along one edge.

- Torsional sliding: Sliding mode associated with a rotation mode.
- Remote axis rotation: Rotation around a remote location to the block

Corner rotation and edge rotation were analysed in this thesis because they show a pure rotational mode. Torsional sliding and remote axis rotation were not considered any further because the determination is not feasible with analytical methods and a comprehensive numerical analysis is necessary.

### 2.2.5.1 Mode analysis

For the determination of the rotation mode the unconstrained motion of the block is considered.

The resultant force and the mass of the block determine the translational acceleration.

$$a_G = \frac{R}{m} \quad (2.22)$$

By means of the inverse of the inertia operator and the moment relative to the centroid it is possible to calculate the angular acceleration  $\dot{\omega}$ . To make this approach possible it has been assumed that the system is at a rest at the beginning of the movement and the initial velocity is equal to zero.

$$\dot{\omega} = \mathbf{E}^{-1} * M_g \quad (2.23)$$

### Corner rotation

The rotational corner is formed by two joint planes and the free face (see figure 2.12). The rotation axis runs through it. Each block has three free corners where the joint planes intersect with the free face.

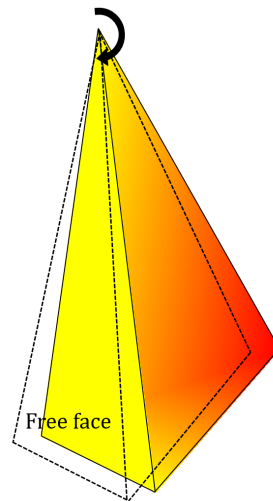


Figure 2.12: Corner rotation around the upper corner

In the first place it is essential to analyse the relationship between the joint planes to each other to see if the block is rotatable due to its geometric shape (see figure 2.13) .

For rotation to occur the angle between two inward planes needs to be obtuse. Therefore the normal vectors need to correlate as follows:

$$\hat{n}_i \cdot \hat{n}_h \geq 0 \text{ or } \hat{n}_i \cdot \hat{n}_j \geq 0 \quad (2.24)$$

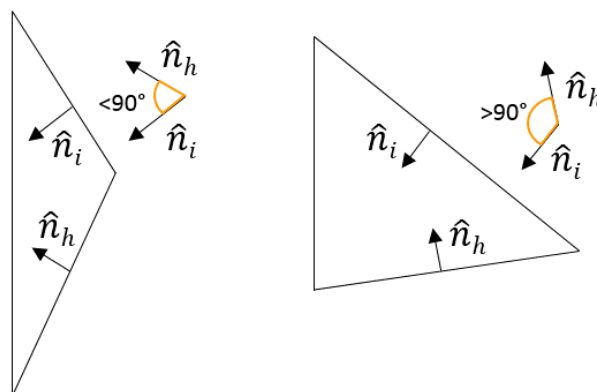


Figure 2.13: Relationship between the joint planes defined by the normal vectors

The vector analysis calculates the dot product of the acceleration values and the normal vectors of the planes. Subsequently conclusions about the angle between the direction of motion of the translational and angular acceleration and the normal vectors can be drawn.

As the direction of the normal vector of the joint planes is known, it is possible to evaluate the direction of the motion.

Figure 2.14 shows the relationship between the normal vectors  $\hat{n}_i$  and  $\hat{n}_h$  of the plane and how the normal vectors change as soon as the angle between the planes increases or decreases.

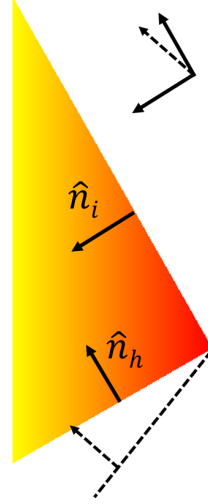


Figure 2.14: Relationship between normal vectors changes if the angle between the joint planes changes

Assuming that the angle conditions of the vectors have been fulfilled the next step is to analyse the motion of the free corners to find out whether one corner tends to move inside the rock mass and two free corners tend to move outside towards the free space. The normal vector of the free face  $\hat{n}_f$  points into the block and thus also into the rock mass.

If, for example, rotation would occur around a corner  $A_i$ , according to Tonon (1998) the equations need to be as follows:

$$\Delta A_i \cdot \hat{n}_f = (a_G + \dot{\omega}_u \times GA_i) \cdot \hat{n}_f > 0 \quad (2.25)$$

$$\Delta A_j \cdot \hat{n}_f = (a_G + \dot{\omega}_u \times GA_j) \cdot \hat{n}_f < 0 \quad (2.26)$$

$$\Delta A_h \cdot \hat{n}_f = (a_G + \dot{\omega}_u \times GA_h) \cdot \hat{n}_f < 0 \quad (2.27)$$

If the conditions are fulfilled the block motion causes a reaction force at corner  $A_i$ , which means that the corner remains static and a rotation around this corner is possible. Therefore the two other corners  $A_j$  and  $A_h$  need to move into the excavated space. The angle between

the vector of the static corner reaction and the normal vector of the free face  $\hat{n}_f$  has to be acute. The angle between the vector of the two rotatable corners and the normal vector of the free face  $\hat{n}_f$  has to be obtuse.

Figure 2.15 shows the normal vectors of the planes and the required acting direction of the vectors due to angular and translational acceleration for a corner rotation around corner  $A_i$ .

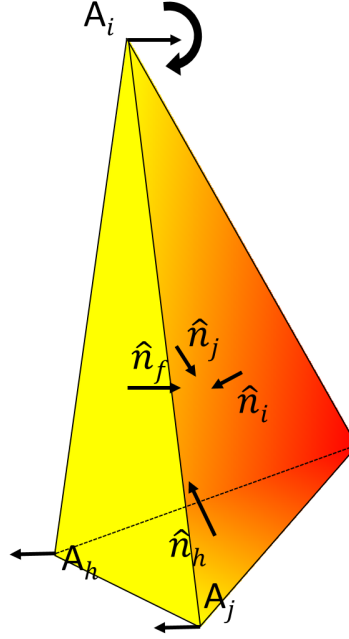


Figure 2.15: Conditions for corner rotation around corner  $A_i$

To conclude the static corner  $A_i$  around which the corner rotation occurs is analysed in regard to the relationship between the acceleration and the normal vector  $\hat{n}_i$  and  $\hat{n}_j$  of the two inward joint planes which intersect the rotation corner. Tonon (1998) verifies the static corner as follows:

$$\Delta A_i \cdot \hat{n}_i = (a_G + \dot{\omega}_u \times GA_i) \cdot \hat{n}_i < 0 \quad (2.28)$$

$$\Delta A_i \cdot \hat{n}_j = (a_G + \dot{\omega}_u \times GA_i) \cdot \hat{n}_j < 0 \quad (2.29)$$

Figure 2.15 shows that the vector of the static corner acts into the opposite direction to the normal vectors  $\hat{n}_i$  and  $\hat{n}_j$  if a rotational mode is possible. Therefore the angle between the vector of the static corner and the normal vectors has to be obtuse.

When all conditions are fulfilled the mode analysis is finished and the calculation continues with the stability analysis. If one condition is not fulfilled corner rotation is not possible.

### Edge rotation

The edge is formed by a joint plane and the free face. It is determined by two adjacent free corners. The rotation axis coincides with the edge (see figure 2.17).

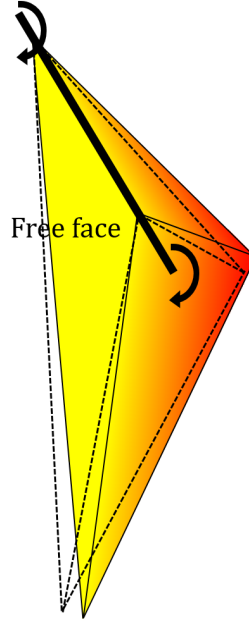


Figure 2.16: Edge rotation with rotation axis in an edge

It is assumed that  $A_i$  and  $A_j$  are the two adjacent free corners of the free edge where the rotation occurs. The edge is defined by the intersection of the free face and a joint plane. For a rotational motion it is necessary that the two corners tend to move inside the rock mass which means that they cause a reaction. The third free corner  $A_h$  tends to move into the excavated space. These circumstances can be expressed as follows (Tonon, 1998):

$$\Delta A_i \cdot \hat{n}_i = (a_G + \dot{\omega}_u \times GA_i) \cdot \hat{n}_i < 0 \quad (2.30)$$

$$\Delta A_j \cdot \hat{n}_j = (a_G + \dot{\omega}_u \times GA_j) \cdot \hat{n}_j < 0 \quad (2.31)$$

$$\Delta A_h \cdot \hat{n}_f = (a_G + \dot{\omega}_u \times GA_h) \cdot \hat{n}_f < 0 \quad (2.32)$$

Figure 2.17 shows the block and its rotational axis.

The vectors of the two static corners  $A_i$  and  $A_j$  act into the rock mass and the normal vector of the inward plane  $\hat{n}_i$  acts in the opposite direction. Therefore the angle between the two vectors has to be obtuse. In contrast the vector of the rotational corner  $A_h$  acts into the

free space whereas the normal vector of the free face acts in the block. This angle has to be obtuse as well.

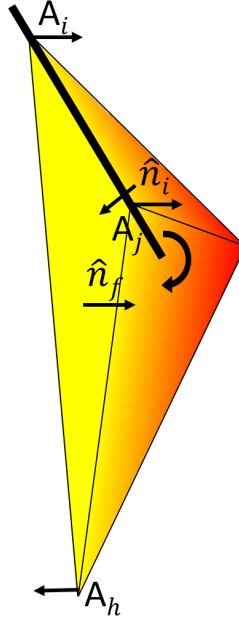


Figure 2.17: Conditions for edge rotation around the corners  $A_i$  and  $A_j$

### 2.2.5.2 Stability analysis

The stability analysis examines the rotation around the static corner which was selected in the mode analysis. Therefore the origin is transferred to the rotation corner. It is important to determine the moment around the rotational corner using the following equation:

$$M_{Ai} = M_g + A_i G \times R \quad (2.33)$$

The coordinates of the vertices also change as the origin is transferred to the rotation corner

$$\begin{aligned} C_1 &= (x_1, y_1, z_1) = (x_1, y_1, z_1) - (x_1, y_1, z_1) \\ C_2 &= (x_2, y_2, z_2) = (x_2, y_2, z_2) - (x_1, y_1, z_1) \\ C_3 &= (x_3, y_3, z_3) = (x_3, y_3, z_3) - (x_1, y_1, z_1) \\ C_4 &= (x_4, y_4, z_4) = (x_4, y_4, z_4) - (x_1, y_1, z_1) \end{aligned} \quad (2.34)$$

As the coordinates of the vertices change the moments of inertia and the products of inertia

need to be recalculated with the revised coordinates by using equation 2.14 and equation 2.15. The inertia operator is then evaluated as follows

$$\mathbf{E}_i = \begin{pmatrix} a_i & -b'_i & -c'_i \\ -b'_i & b_i & -a'_i \\ -c'_i & -a'_i & c_i \end{pmatrix} \quad (2.35)$$

By solving the inertia operator with the revised coordinates it is possible to determine the value of the angular acceleration again.

$$\dot{\omega} = \mathbf{E}_i^{-1} * M_{A_i} \quad (2.36)$$

### Corner rotation

Each point except corner  $A_i$  detaches from the rock mass. As a consequence no frictional forces are applied on the block. To proof if all points except corner  $A_i$  detach and the block rotates around the corner the following equation needs to be fulfilled:

$$\dot{\omega} \times A_i A_j \cdot \hat{n}_i \geq 0 \quad q \in S_{A_j}; \quad j = 1, \dots, 4 \quad j \neq i \quad (2.37)$$

Corner  $A_j$  is any free corner different from  $A_i$  and  $\hat{n}_i$  is the inward normal to the face bordered by the rotational edge. If one inequality is not fulfilled rotation is kinematically not possible and a translational failure may occur.

### Edge rotation

The angular acceleration  $\dot{\omega}$  has to coincide with the rotational edge  $A_i A_j$  and is subject to the moment around one free corner along the edge.

$$\dot{\omega} = (M_{A_i} \cdot A_i A_j) A_i A_j \quad (2.38)$$

Assuming that the angular acceleration  $\dot{\omega}$  is equal to zero the block would be at limit equilibrium. To find out if the block is pushed against the rock mass or towards the free space it is decisive to take a look at the motion of the corner  $A_4$  inside the rock mass. The normal vector  $\hat{n}_i$  belongs to the inward plane adjacent to the rotational edge.

- If

$$(\dot{\omega} \times A_i A_4) \cdot \hat{n}_i < 0 \quad (2.39)$$

the block is stable against edge rotation.

- If

$$(\dot{\omega} \times A_i A_4) \cdot \hat{n}_i > 0 \quad (2.40)$$

the block is unstable and rotates into the free space of the excavation.

Once the investigation is completed it is possible to draw conclusions about the kind of failure that might occur or whether the block is stable.

## 2.3 Numerical analysis of tunnel face instabilities

The numerical analysis was done with the software 3DEC (Itasca, 2013). The software allows a three-dimensional numerical calculation of the blocks with the distinct element method (DEM).

According to the manual (Itasca, 2013) the software calculates the motion in a simplified way compared to the block theory analysis.

The software derives the translational motion with the following equation:

$$\ddot{x}_i + \alpha \dot{x}_i = \frac{F_i}{m} + g_i \quad (2.41)$$

where  $\ddot{x}_i$  is the acceleration of the block centroid,  $\dot{x}_i$  is the velocity of the block centroid,  $\alpha$  is the viscous (mass-proportional) damping constant,  $F_i$  is the sum of forces applied to the block,  $m$  is the mass of the block and  $g_i$  is the gravity acceleration vector.

The rotational motion is described by only the moments of inertia and the corresponding angular velocity components and not with an inertia operator. For this equation the angular velocity  $\omega_i$  is also a component.

$$\begin{aligned} I_1 \dot{\omega}_1 + (I_3 - I_2) \omega_3 \omega_2 &= M_1 \\ I_2 \dot{\omega}_2 + (I_1 - I_3) \omega_1 \omega_3 &= M_2 \\ I_3 \dot{\omega}_3 + (I_2 - I_1) \omega_2 \omega_1 &= M_3 \end{aligned} \quad (2.42)$$

3DEC (Itasca, 2013) simplifies the calculation by determining an approximate moment of inertia. The manual considers the inertia operator as not essential because inertial forces are small compared to the total forces acting to the block.

## 3 Block stability analysis using analytical and numerical methods

The behaviour of blocks was analysed using both analytical and numerical methods. Block geometries were derived from the tunnel face documentation at KAT2. These blocks were systemically analysed by the methods outlined in chapter 2. The results of block theory and 3DEC (Itasca, 2013) were compared.

### 3.1 Results of block theory

The application of block theory for block failure was carried out with the program MATLAB (MathWorks, 2016). The vector analysis was executed by means of two scripts - one for the translational analysis and one for the rotational analysis. The input parameters are trend and plunge of the three joint planes, the normal distance from the origin, the unit weight of the rock mass, average cutter force and the friction angle. In addition it is necessary to specify the halfspaces of joint planes which form the block.

First of all the normal vectors and the geometry of the block are calculated. The coordinates of the block are examined with respect to the shape and size conditions. As soon as the geometric conditions are fulfilled the block theory analysis is carried out. The different steps are built on each other and the script displays the intermediate results stepwise to finally identify whether the block is stable or whether failure occurs. Furthermore the software displays the block and its position in the tunnel face. The illustrations in MATLAB (MathWorks, 2016) are also a reliable resource to understand the vector analysis with respect to the direction of the normal vectors of the planes and the block displacement vectors.

At the beginning the idealized blocks for corner rotation and edge rotation were simulated to find out if failure is generally possible. The idealized blocks have the perfect conditions for

a rotational failure regarding their shape and the applied forces. The results are described below.

### 3.1.1 Corner rotation

The optimum conditions were analysed to simulate the possibility of rotational failure. It is important that the size of the block is maximized to increase the weight. Moreover it is necessary to take into account that the angles between two inward planes have to be obtuse.

In addition, the contact point of the applied cutter force is essential. According to Gehring (1995) the cutter force is estimated at 200 kN for each disk cutter. This parameter serves as a mean value for the disks distributed over the cutter head. Other studies refer to larger disk loads up to more than 400 kN (Entacher & Galler, 2013). For this thesis the maximum load was considered at 200 kN. Since this thesis deals with movements into the excavated space the extreme case of 400 kN is not evaluated.

Figure 3.1 shows the ideal block for corner rotation to occur when the cutter force is applied with 200 kN. The bold line represents the excavation perimeter and the thin line represent the path of the cutter force. A "x" marks the contact point of the cutter force on the block. The excavation radius was assumed with 5 m. This block shows that corner rotation takes place while the block is stable against sliding.

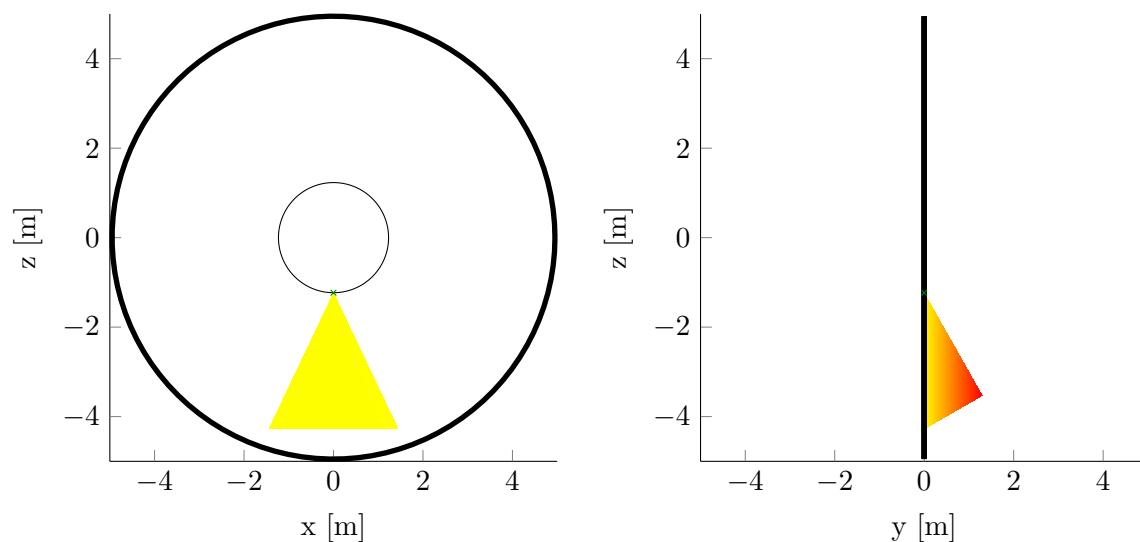


Figure 3.1: Ideal block shape for corner rotation with an applied cutter force of 200 kN

Although the conditions for rotation are fulfilled, the block might be fixed to its position

due to the type of construction of the tunnel boring machine. In case of the TBM at the construction site of KAT2 the block could not rotate due to the arrangement of the disk cutters. Figure 3.2 shows the cutter head at KAT2 and the block is highlighted in red. Even though a disk cutter could provoke a rotation the block is stabilized by other disk cutters that are in contact with the block practically simultaneously because the distance between different disks is limited. The block is hindered in its rotational motion and might damage the disk cutters that stabilise the block.

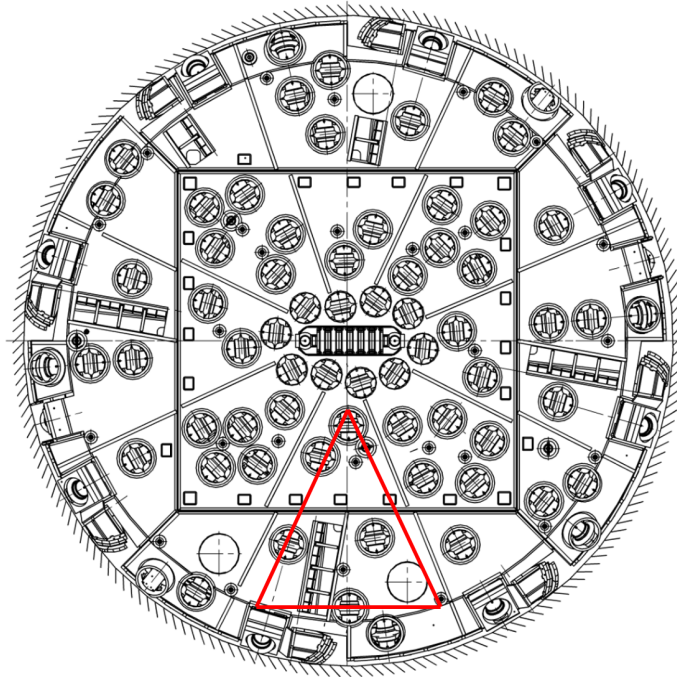


Figure 3.2: Cutter head of the TBM at KAT2 and block for the rotation analysis

If the block size is decreased to an appropriate size the applied force needs to be decreased for rotational failure because the dead weight of the block is reduced.

Since different tunnel boring machines have different designs of the cutter head a motion due to rotation might occur for a block this size because the disks are arranged in a different order.

### 3.1.2 Edge rotation

The possibility of an edge rotation was determined by calculating a block with optimum properties as it was done for corner rotation. Figure 3.3 shows the properties of the idealized block and the position of the block in the tunnel face.

At first the cutter force was applied with 200 kN at the edge where it intersects with the rotational axis. The block shows a stable behaviour against sliding and rotation. After decreasing the cutter force to zero the block is still stable. A proper analysis of the calculation reveals that a force acting into the excavated space is necessary for a rotational motion around an edge.

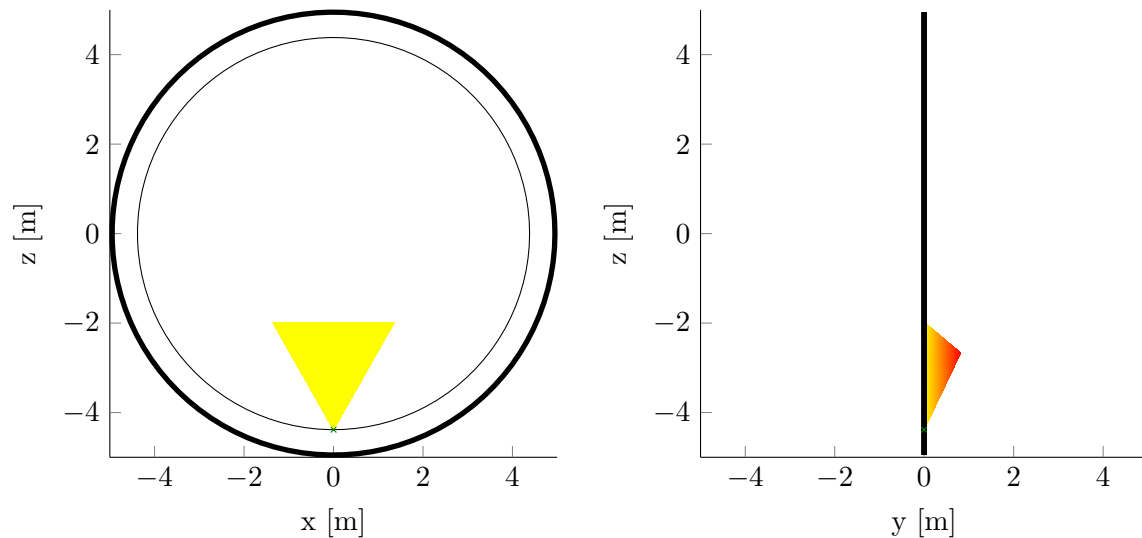


Figure 3.3: Ideal block shape for edge rotation

The analysis of edge rotation can be explained with the relationship between the angular acceleration of the block and the plunge of the inward joint plane intersecting with the rotational edge. As shown in figure 3.4 the angular acceleration  $\dot{\omega}$  coincides with the rotation edge. The cross product of the angular acceleration and the normal vector of the inward joint plane  $A_i$  and  $A_4$  results in a vector perpendicular to both vectors. The acting direction of this vector depends on the direction of the resultant force. If the resultant force acts into the excavated space, the vector also acts into the free space.

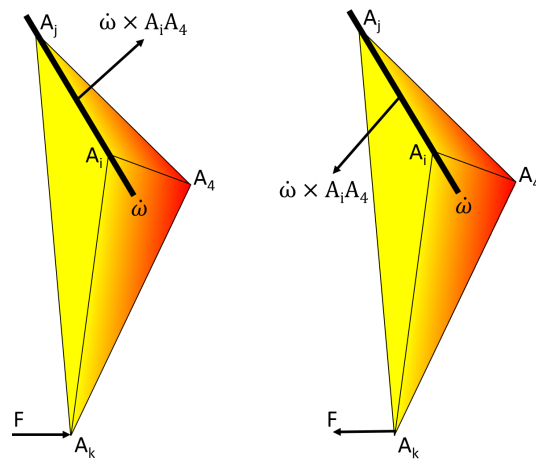


Figure 3.4: Edge rotation depends on the acting direction of the cutter force

This condition can be justified with an unbalanced reaction force. While the cutter force and the dead weight of the block are acting a reaction force develops at the inward joint planes (see figure 3.5). As a consequence the reaction force creates a state of equilibrium. When the cutter force leaves the block the forces are redistributed and the residual forces are the dead weight and the reaction force. Due to the sudden removal of the cutter force an impact takes place, which creates a virtual force acting into the excavated space. The impact acts for a short time and was assumed to be elastic which means that the entire cutter force was estimated to act into the excavated free space. The principle of linear momentum implies that the total momentum is constant in a closed system.

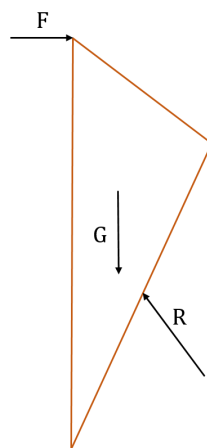


Figure 3.5: State of equilibrium with the acting forces

Thus special circumstances are necessary for a rotational motion around an edge, this case was not taken into consideration for the further case study.

## 3.2 Numerical simulation of block failure in 3DEC (Itasca, 2013)

The ideal blocks for corner and edge rotation were additionally analysed with the software 3DEC (Itasca, 2013) to verify the results of the analytical solution. The parameters for the shape and size of the blocks were the same as for the analytical calculation with block theory. Furthermore material parameters for the normal stiffness, the shear stiffness and the friction angle of the joints were added. As the block is rigid the only material parameter of the block is the density.

### 3.2.1 Corner rotation in 3DEC (Itasca, 2013)

The corner rotation was executed with a block of the same geometric dimensions as the simulated block in MATLAB (MathWorks, 2016). The applied force from the cutter acts in the upper corner. Figure 3.6 illustrates the block formed by the joint planes.

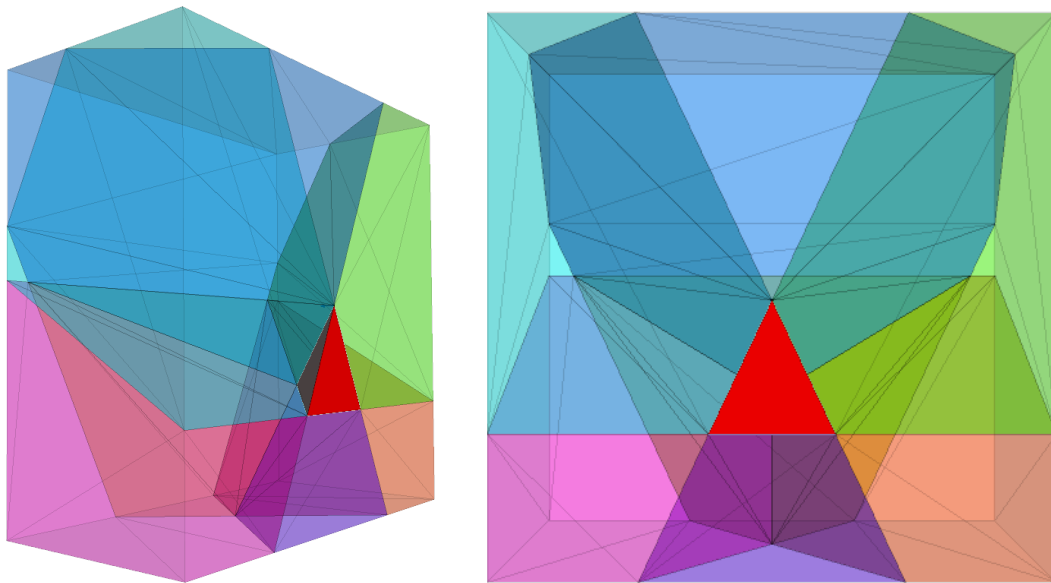


Figure 3.6: Ideal block for corner rotation highlighted in red

The basic requirement for corner rotation to occur is to neglect the friction angle and the cohesion. Figure 3.7 shows the process of corner rotation. At the beginning of rotation the corner is still fixed to its position due to the applied cutter force. This process confirms the vector analysis where the rotational corner is fixed during the rotational motion and the two opposite corners move into the free space. After a certain time the dead load shifts the

block downwards. As the block moves, the point where the cutter force was applied shifts also downwards. In 3DEC (Itasca, 2013) it is not possible to fix the point to its position when the block is rigid. In contrast, the block theory analysis works with a block whose rotational corner is fixed to its position during the entire rotational motion. 3DEC (Itasca, 2013) combines the sliding and the rotational motion, whereas the analytical calculation allows either sliding or rotation.

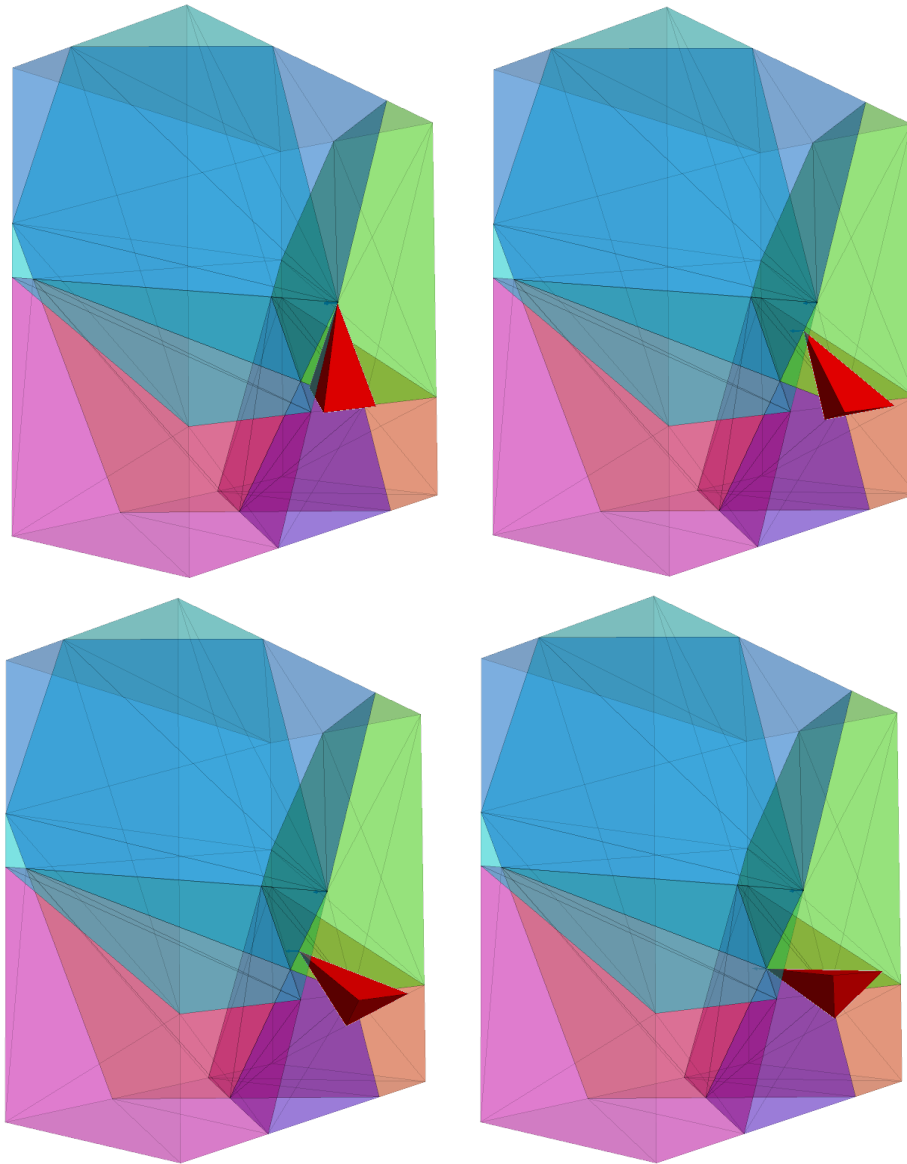


Figure 3.7: Rotation around the upper corner

### 3.2.2 Edge rotation in 3DEC (Itasca, 2013)

The idealized block for edge rotation was also simulated in 3DEC (Itasca, 2013). Figure 3.8 shows the block in terms of its geometric shape.

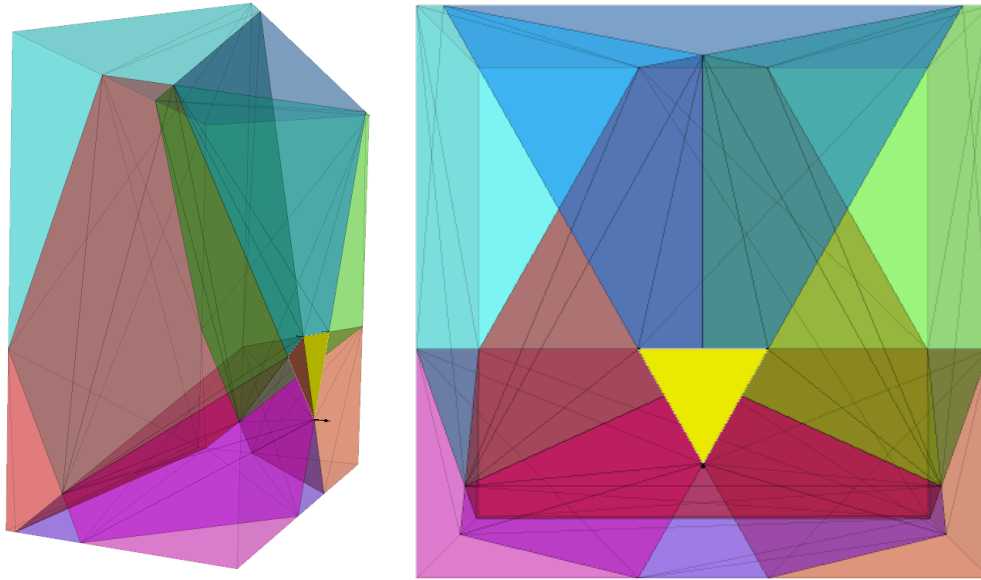


Figure 3.8: Ideal block for edge rotation highlighted in yellow

The applied forces are the dead load and the cutter force. Due to these forces a reaction force develops at the lower joint planes as already mentioned in chapter 3.1.2. In 3DEC this reaction force is applied immediately after the cutter force leaves the block at the lower corner, which pulls the block into the excavated space. On the basis of the principle of linear momentum the force acting into the free space complies with the cutter force which is the remaining force. Therefore gravity is neglected. After the emerged impact had been released, the dead load is applied and the reaction force is decreased to zero. Figure 3.9 shows the block moving into the excavated space. The later applied cutter force has only a small impact on the motion of the block.

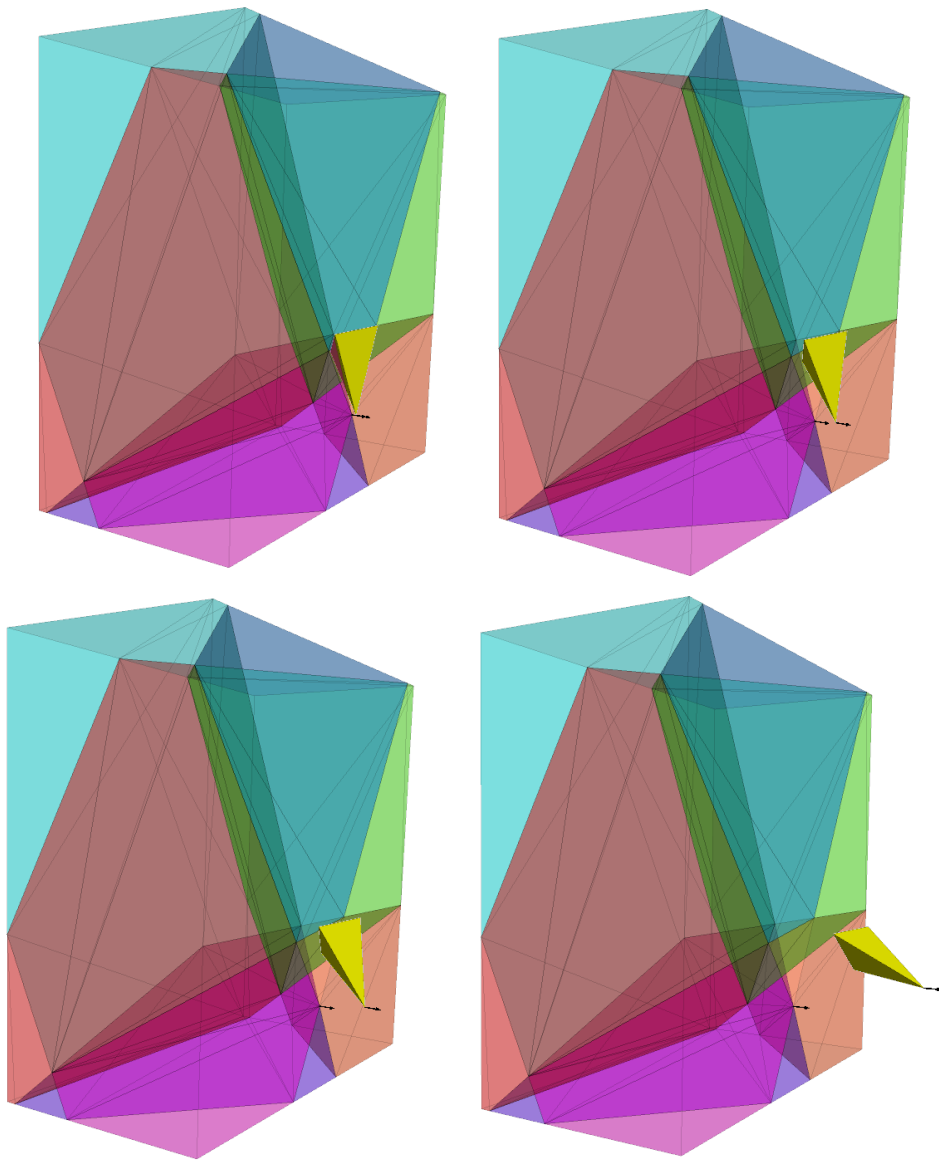


Figure 3.9: Rotation around the upper edge

### 3.3 Case study based on the 3D tunnel face documentation

A case study was performed with the structural parameters obtained from the 3D images of KAT2, generated with the software ShapeMetriXTBM (3GSM, 2016). Therefore, detached tetrahedral blocks from the tunnel faces were analysed with analytical and numerical methods of computation.

For the case study the tunnel faces were analyzed with respect to tetrahedral blocks which fulfil the conditions for block theory.

The following load situations were investigated:

- Load case 1: Dead load of the block
- Load case 2: Dead load of the block and cutter force applied with 200 kN at a corner

The blocks were analysed with respect to sliding and corner rotation.

#### 3.3.1 Tunnel face at chainage 14321.13 m

As shown in figure 3.10 the foliation and joint sets form tetrahedral blocks. Close to the left side wall a block has detached from the tunnel face. According to the documentation the tunnel face shows tapered blocks until a depth of 0.5 m along the slickensides and joints. Although several blocks detached the left block has been used for the exemplary calculation.

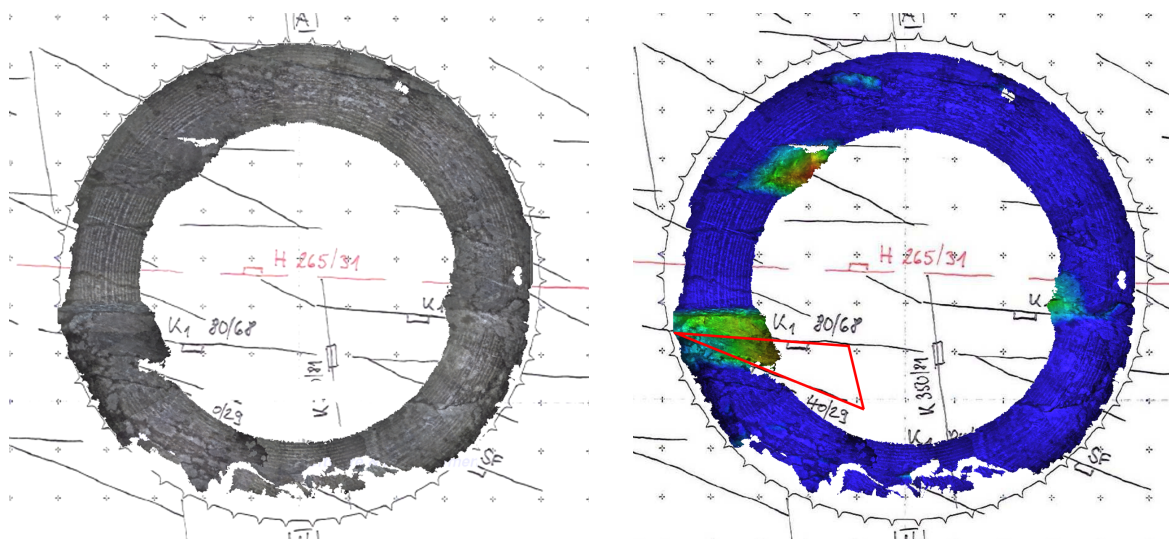


Figure 3.10: 3D image of the tunnel face at chainage 14321.13 m and topographic map of the tunnel face with the detached block highlighted in red

Figure 3.11 shows the analysis results of block theory. In load case 1 the block is stable due to sliding and rotation. After increasing the cutter force the block is still stable against sliding due to friction. For rotation around the left corner the mode analysis would allow rotation. The block is stable in terms of the complete stability analysis.

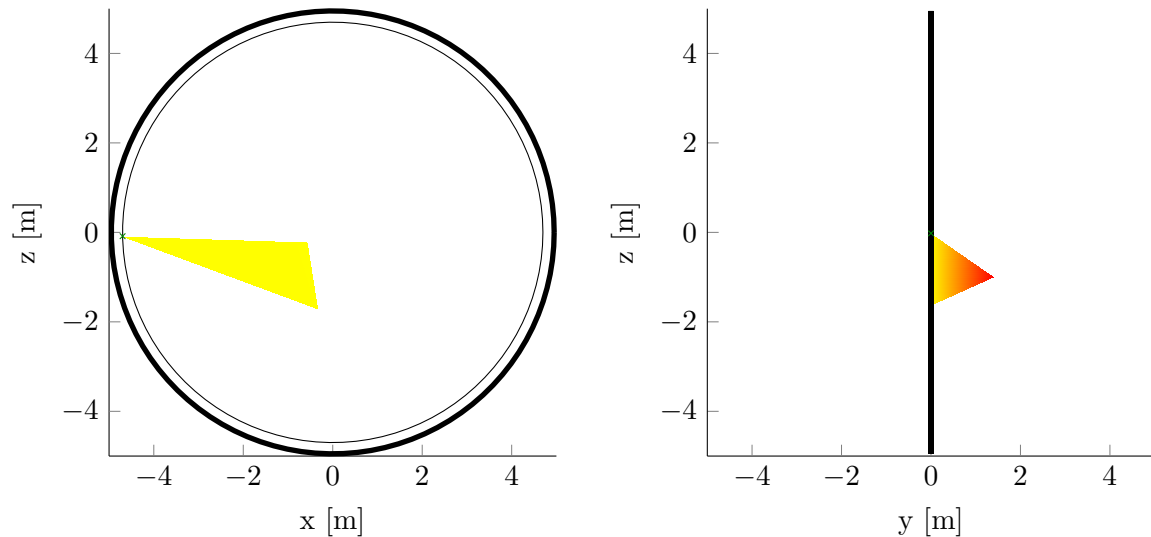


Figure 3.11: Analysis of a tetrahedral block at chainage 14321.13 m

The numerical simulation in 3DEC (Itasca, 2013) confirms that the block is stable due to sliding and rotation for load case 1. When the cutter force was applied in the left corner of the block for load case 2 a rotational failure occurred. As the corner is not fixed and a horizontal shifting takes place the rotation behaves differently from the calculation with vector analysis. Figure 3.12 shows the rotation around the corner.

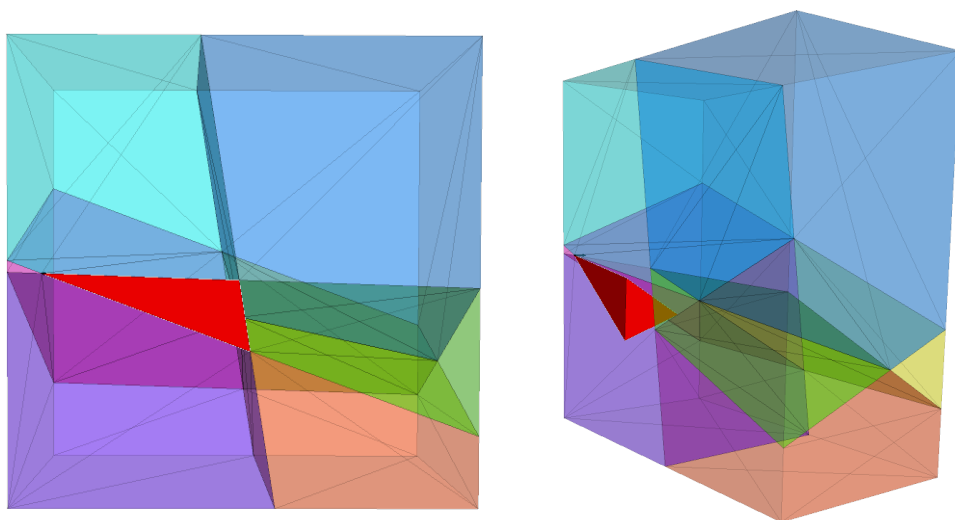


Figure 3.12: Numerical simulation of a tetrahedral block (red) at chainage 14321.13 m

### 3.3.2 Tunnel face at chainage 14335.46 m

Figure 3.13 shows that the tunnel face is located in a fault zone and plenty of blocks have detached from the tunnel face. Moulds of detached blocks along fault zones and slickensides are approximately 1.5 m deep.

The tunnel face documentation shows a tetrahedral block situated in the centre of the face. From the 3D image it is not obvious if the block detached from the face.

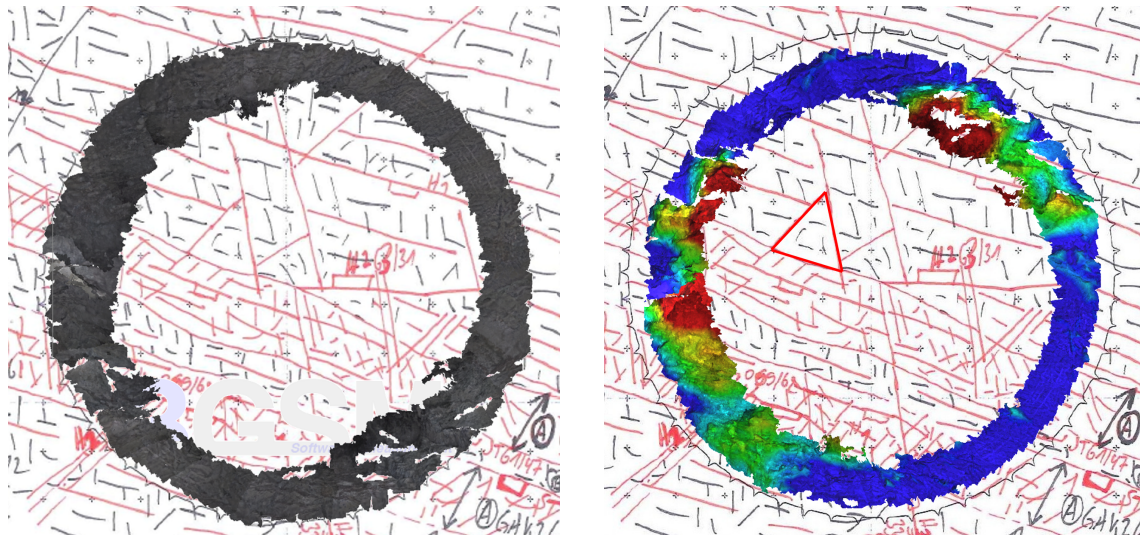


Figure 3.13: 3D image of the tunnel face at chainage 14335.46 m and topographic map of the tunnel face with the detached block highlighted in red

In the first load case the dead weight of the block generates a sliding motion. Therefore sliding is possible although the block is stable against rotational failure.

After applying the cutter force neither sliding nor rotation occurs as the applied cutter force stabilises the block. Figure 3.14 shows the block in the tunnel face at chainage 14335.46 m calculated in MATLAB (MathWorks, 2016).

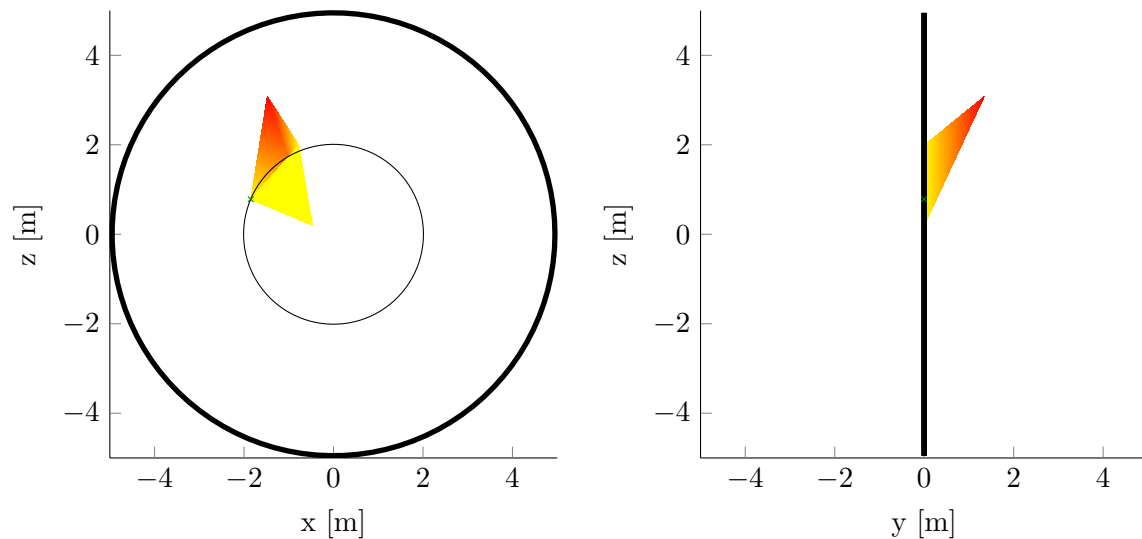


Figure 3.14: Analysis of a tetrahedral block at chainage 14335.46 m

The numerical simulation also allows sliding in the initial state due to the dead weight. After applying the cutter force with 200 kN in one corner, the block is stable against sliding and rotation. The results of the analytical and the numerical calculation coincide. Figure 3.15 shows the block in 3DEC (Itasca, 2013) during the sliding process for load case 1.

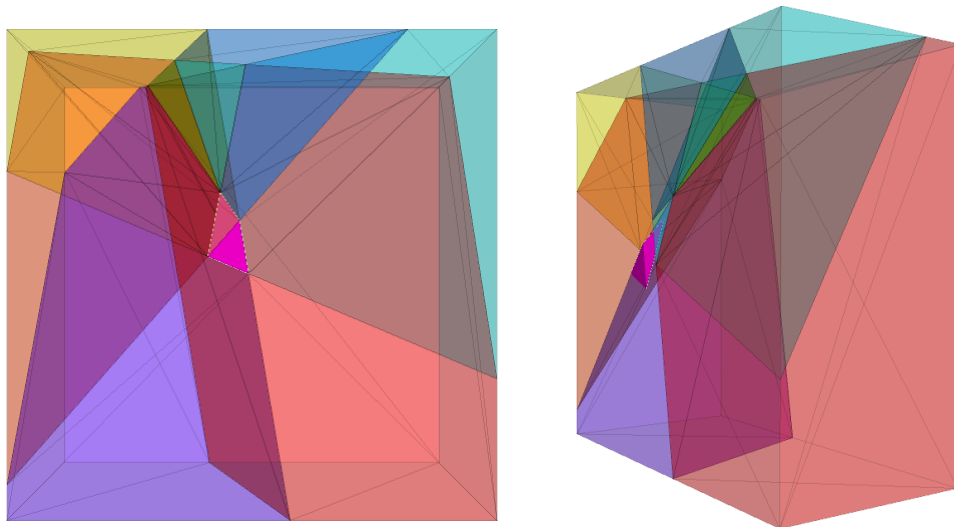


Figure 3.15: Numerical simulation of a tetrahedral block (pink) at chainage 14335.46 m

### 3.3.3 Tunnel face at chainage 14660.39 m

The tunnel face at chainage 14660.39 m shows several instabilities. Especially in the upper left sector the tunnel face reveals moulds of detached blocks along joint planes. A fault zone

and a slickenside run parallel to the foliation in the upper sector. Figure 3.16 shows that a block in the left sector detached from the face. The parameters for plunge and trend from the tunnel face documentation indicate that the detached block is tetrahedral and therefore suitable for the calculation.

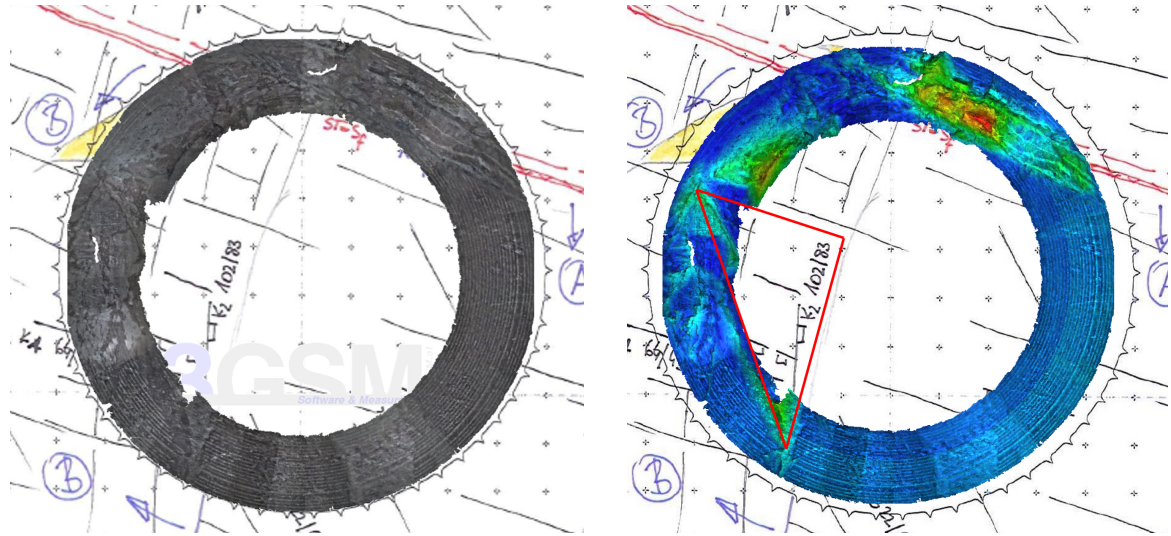


Figure 3.16: 3D image of the tunnel face at chainage 14660.39 m and topographic map of the tunnel face with the detached block highlighted in red

The input parameters from the manual tunnel face documentation deviate from the 3D image. Therefore the determined block geometry does not correspond to the one observed in the 3D image (see figure 3.17). In load case 1 the block was stable against rotation. The calculation showed a sliding mode on two joint planes.

At an applied cutter force the block was stabilised and neither sliding nor rotation was possible.

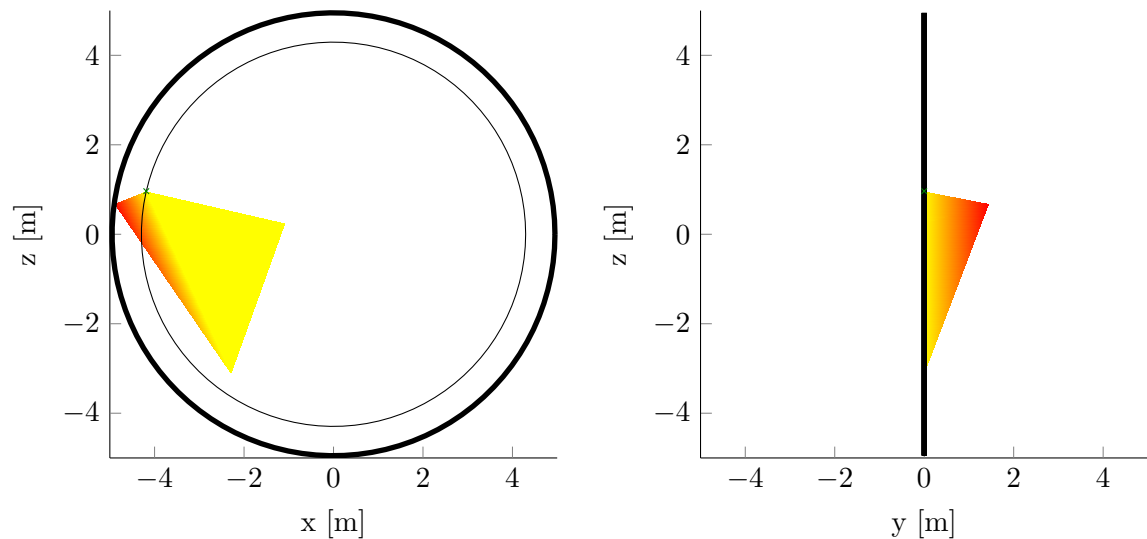


Figure 3.17: Analysis of a tetrahedral block at chainage 14660.39 m

The results from the vector analysis correspond to the numerical simulation in 3DEC (Itasca, 2013). The block slides on two joint planes when no cutter force is applied. Due to the orientation of the joint planes the friction decelerates the motion. After the cutter force is applied, the block is stable against sliding and rotation. Figure 3.18 shows the block during the sliding process in the initial state for load case 1.

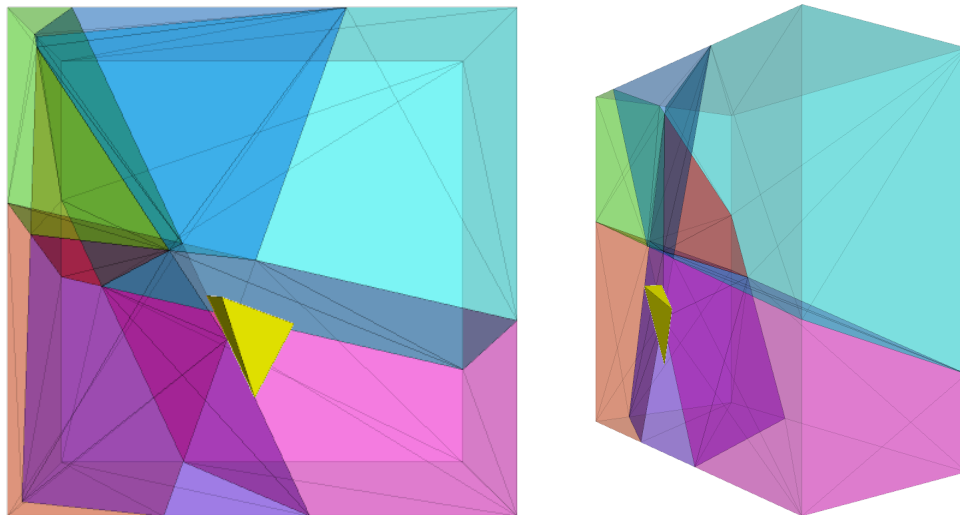


Figure 3.18: Numerical simulation of a tetrahedral block (yellow) at chainage 14660.39 m

### 3.3.4 Tunnel face at chainage 14703.07 m

Figure 3.19 shows that this tunnel face is stable except for a detached block in the left, lower sector with a depth of 0.3 m. The tunnel face documentation indicates that the block is tetrahedral.

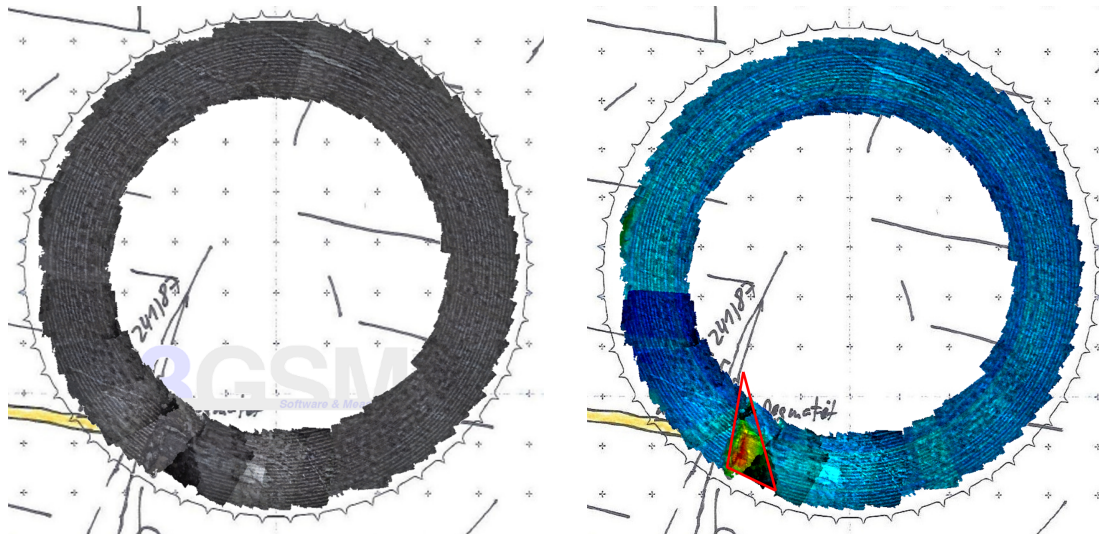


Figure 3.19: 3D image of the tunnel face at chainage 14703.07 m and topographic map of the tunnel face with the detached block highlighted in red

The shape of the block was also defined by the input parameters based on the tunnel face documentation (see figure 3.20). For load case 1 the block is stable against sliding and rotation. Sliding is hindered by friction.

For load case 2 the block is still stable. The cutter force has a stabilising impact on the block. The mode analysis would allow rotation at the upper corner. The block is stable due to the final step of the stability analysis.

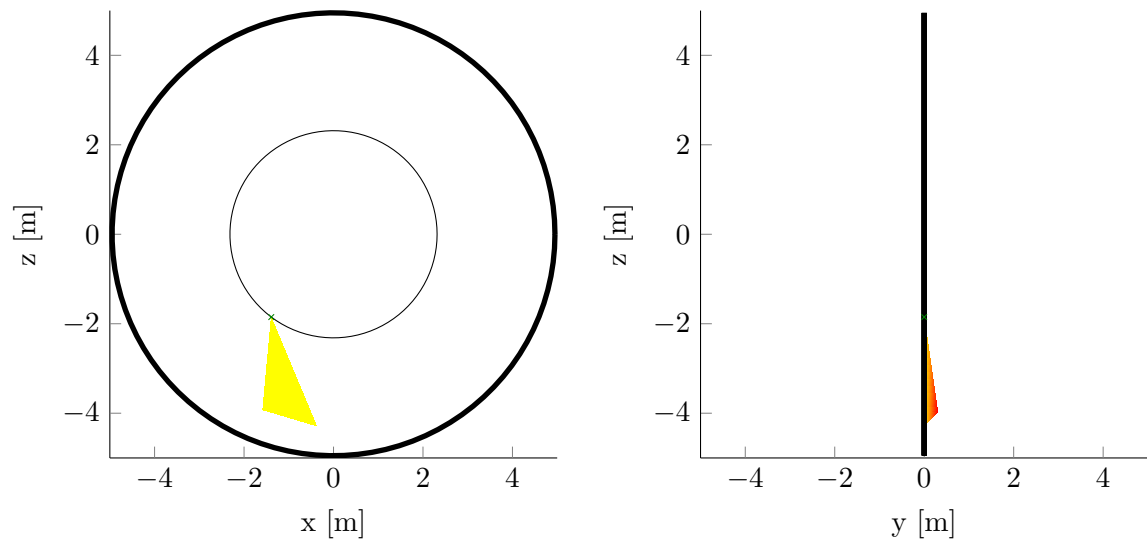


Figure 3.20: Analysis of a tetrahedral block at chainage 14703.07 m

In 3DEC (Itasca, 2013) the block is stable by sufficient friction as long as the cutter force does not penetrate the surface. When the force is applied with 200 kN at the upper corner the block is moved and a combination of sliding and rotation shifts the block downwards and destabilises it.

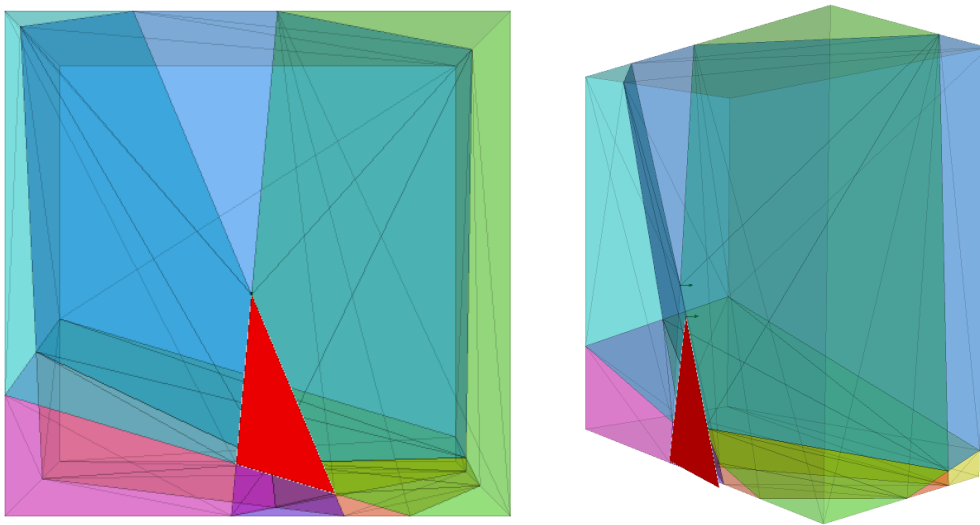


Figure 3.21: Numerical simulation of a tetrahedral block (red) at chainage 14703.07

## 4 Conclusion and Outlook

The aim of the work was the determination of failure behaviour of blocks from a tunnel face when excavating with a tunnel boring machine. With the help of 3D tunnel face documentation detached blocks were localized in a tunnel face and their failure was analysed regarding rotation and sliding based on a vector analysis.

At first 3D images were generated with the software ShapeMetriXTBM (3GSM, 2016) developed by 3GSM. These images are derived from videos taken with an imaging unit in one of the inspection openings in the cutter head of a TBM. The unit creates a video of the visible part of the tunnel face and records orientation data. Afterwards overlapping single frames, extracted from the video, are generated to an annular 3D image. This image allows conclusions regarding the planarity of the actual tunnel face and shows moulds of detached blocks. Within a research project at the construction site of KAT2 20 three-dimensional tunnel face images were generated.

The 3D images show moulds of detached blocks in the tunnel faces, the failure behaviour of the detached blocks however is unknown. Therefore, the blocks were analysed by means of a vector analysis based on block theory implemented with the software MATLAB (MathWorks, 2016). Additionally the results were compared to a numerical simulation in 3DEC (Itasca, 2013). The surveyed failure modes were sliding along one or two joint planes and rotation around a corner or an edge. To simplify the calculation the analysed blocks were defined as rigid and tetrahedral. The acting forces result from the dead weight of the block and an average cutter force which acts on the tunnel face.

An in-depth investigation of the sliding failure showed that this motion is only possible when the cutter force is neglected. In this case the initial state is examined when the only acting force results from the dead weight of the block.

A rotational failure around a corner is possible with a cutter force acting at the rotational corner of the block and causing a rotational movement around that corner. In contrast, edge

rotation might occur only with a force pointing into the free space in the opposite direction to the cutter force. This force could be represented with the reaction component that allows a state of equilibrium while cutter force and dead load are operating. Immediately after the disk cutter leaves the surface of the block the remaining reaction force induces a rotational movement into the free space of the excavation. A numerical analysis of the inward joint plane where the reaction force develops could give specific information about the stresses. Thus the conditions for edge rotation could be defined more precisely.

Subsequently the theoretical calculation was applied to the 3D tunnel face images from KAT2. Therefore a case study was provided analytically in MATLAB (MathWorks, 2016) and numerically in 3DEC (Itasca, 2013). The input parameters for the joints were taken from the tunnel face documentation and the cutter force was assumed with an average cutter force of 200 kN.

For the determination of a sliding failure the results of the analytical and the numerical calculation coincide. The comparison between the simulation for rotational failure displays discrepancies. The numerical simulation shows a more realistic behaviour as it is possible to combine sliding and rotation. When using numerical software the procedure to calculate the behaviour is unknown. Therefore the analytical calculation is a good method to verify the numerical results.

The results show that blocks could move due to rotation although they are stable against sliding. This fact results from the eccentric cutter force which acts into the rock mass and induces an active moment.

The thesis hopefully contributes to a better understanding of the interaction between the blocks at the tunnel face and the disc cutters of a TBM.

---

## Bibliography

- 3GSM (2016). *Benutzerhandbuch ShapeMetriXTBM*. Graz: 3GSM.
- Entacher, M. & Galler, R. (2013). Development of a disc cutter force and face monitoring system for mechanized tunnelling / Ortsbrustmonitoring und Leistungsprognose bei TBM-Vortrieben. *Geomechanics and Tunnelling*, 6(6), 725–731.
- Gaich, A. & Pötsch, M. (2016). 3D images for digital tunnel face documentation at TBM headings - Application at Koralmtunnel lot KAT2 / 3D-Bilder zur digitalen Ortsbrustdokumentation bei TBM- Vortrieben - Anwendung beim Koralmtunnel Baulos KAT2. *Geomechanics and Tunnelling*, 9(3), 210–221.
- Gehring, K. (1995). Leistungs- und Verschleißprognosem im maschinellen Tunnelbau. *Felsbau*, 1995(6), 439–448.
- Goodman, R. E. & Shi, G.-h. (1985). *Block theory and its application to rock engineering*. Prentice-Hall international series in civil engineering and engineering mechanics. Englewood Cliffs: Prentice-Hall.
- Harer, G., Mussger, K., Hochgatterer, B., & Bopp, R. (2008). Considerations for Development of the Typical Cross Section for the Koralm Tunnel. *Geomechanik und Tunnelbau*, 1(4), 257–263.
- Irschara, A., Hoppe, C., Bischof, H., & Kluckner, S. (2011). Efficient structure from motion with weak position and orientation priors. In *2011 IEEE Computer Society Conference on Computer Vision and Pattern Recognition Workshops (CVPR Workshops)*, (pp. 21–28).
- Itasca (2013). *Users Guide*. Minneapolis: Itasca Consulting Group Inc.
- Kuypers, F. (1997). *Klassische Mechanik* (5., überarb. Aufl. ed.). Weinheim: Wiley-VCH.

- MathWorks (2016). *MATLAB Primer: Version 9.1* (27 ed.). Natick, Massachusetts: The MathWorks, Inc.
- Pötsch, M. (2011). *The analysis of rotational and sliding modes of failure for slopes, foundations, and underground structures in blocky, hard rock: Techn. Univ., Diss. Graz, 2011*, volume 42 of *Gruppe Geotechnik Graz / Technische Universität Graz*. Graz: Techn. Univ.
- Tonon, F. (1998). Generalization of Mauldons and Goodmans Vector Analysis of Keyblock Rotations. *Journal of Geotechnical and Geoenvironmental Engineering, Issue 10*(Vol. 124), 913–922.